THE ASTROPHYSICAL JOURNAL, 463:254–270, 1996 May 20

THE α CENTAURI LINE OF SIGHT: D/H RATIO, PHYSICAL PROPERTIES OF LOCAL INTERSTELLAR GAS, AND MEASUREMENT OF HEATED HYDROGEN (THE "HYDROGEN WALL") NEAR THE HELIOPAUSE[1]

JEFFREY L. LINSKY[2] AND BRIAN E. WOOD[2]

Received 1995 September 5; accepted 1995 December 4

ABSTRACT

We analyze high-resolution spectra of the nearby (1.34 pc) stars α Cen A (G2 V) and α Cen B (K1 V), which were obtained with the Goddard High Resolution Spectrograph on the *Hubble Space Telescope*. The observations consist of echelle spectra of the Mg II 2800 Å and Fe II 2599 Å resonance lines and the Lyman-α lines of hydrogen and deuterium. The interstellar gas has a velocity ($v = -18.0 \pm 0.2$ km s^{-1}) consistent with the local flow vector proposed for this line of sight by Lallement & Bertin (1992). The temperature and nonthermal velocity inferred from the Fe II, Mg II, and D I line profiles are $T = 5400 \pm 500$ K and $\xi = 1.20 \pm 0.25$ km s^{-1}, respectively. However, single-component fits to the H I Lyman-α lines yield a Doppler parameter ($b_{\rm H\,I} = 11.80$ km s^{-1}) that implies a significantly warmer temperature of 8350 K, and the velocity of the H I absorption ($v = -15.8 \pm 0.2$ km s^{-1}) is redshifted by about 2.2 km s^{-1} with respect to the Fe II, Mg II, and D I lines. The one-component model of the interstellar gas suggests $\log N_{\rm H\,I} = 18.03 \pm 0.01$ and D/H = $(5.7 \pm 0.2) \times 10^{-6}$. These parameters lead to a good fit to the observed spectra, but this model does not explain the higher temperature and redshift of H I relative to the other interstellar lines.

The most sensible way to resolve the discrepancy between H I and the other lines is to add a second absorption component to the H I lines. This second component is hotter ($T \approx 30{,}000$ K), is redshifted relative to the primary component by 2–4 km s^{-1}, and has a column density too low to be detected in the Fe II, Mg II, and D I lines. We propose that the gas responsible for this component is located near the heliopause, consisting of the heated H I gas from the interstellar medium that is compressed by the solar wind. This so-called "hydrogen wall" is predicted by recent multifluid gasdynamical models of the interstellar gas and solar wind interaction. Our data provide the first measurements of the temperature and column density of H I in the hydrogen wall. After considering the effects that a corresponding hydrogen wall around α Cen would have on our analysis, our best estimates for the parameters of the solar hydrogen wall are $\log N_{\rm H\,I}^{(2)} = 14.74 \pm 0.24$, $b_{\rm H\,I}^{(2)} = 21.9 \pm 1.7$ km s^{-1} (corresponding to $T = 29{,}000 \pm 5000$ K), and $v_{\rm H\,I}^{(2)} > -16$ km s^{-1}.

Unfortunately, the existence of this heated H I reduces our ability to compute the H I column density of the interstellar medium accurately because, with slight alterations to our assumed stellar Lyman-α profiles, we discovered that acceptable two-component fits also exist with $\log N_{\rm H\,I} \sim 17.6$. We, therefore, quote large error bars for the H I column density along the α Cen line of sight, $\log N_{\rm H\,I} = 17.80 \pm 0.30$. For this range in $N_{\rm H\,I}$, $n_{\rm H\,I} = 0.15$ cm^{-3} (± a factor of 2) and D/H = $(0.5\text{–}1.9) \times 10^{-5}$. This is the first direct measurement of the H I density in a local cloud and allows us to predict the distance from the Sun to the edge of the local cloud along various lines of sight. This range in D/H is consistent with the value D/H = 1.6×10^{-5} previously derived for the Capella and Procyon lines of sight. We cannot tell whether the D/H ratio varies or is constant in the local interstellar medium, but we do find that the D I/Mg II ratio for the α Cen line of sight is about 4 times smaller than for the Capella and Procyon lines of sight. Therefore, either D/H or the Mg depletion varies significantly over distance scales of only a few parsecs.

Subject headings: ISM: abundances — ISM: kinematics and dynamics — radio lines: ISM stars: individual (α Centauri) — ultraviolet: ISM

1. INTRODUCTION

We analyze in this paper our Goddard High Resolution Spectrograph (GHRS) observations of interstellar gas absorption along the line of sight toward both components of the α Cen visual binary system—α Cen A (G2 V) and α Cen B (K1 V). Our objective was to measure very accurately the cosmologically important deuterium/hydrogen (D/H) ratio in a very short (1.34 pc) line of sight that we anticipated should have rather simple and homogeneous physical properties. This program is one component of a larger study of D/H in the local interstellar medium (LISM). Our previous studies of the 12.5 pc line of sight toward Capella (Linsky et al. 1993, hereafter Paper I) and the 3.5 pc line of sight toward Procyon (Linsky et al. 1995, hereafter Paper II) led us to conclude that D/H = (1.6 ± 0.09 [and +0.05, −0.10 systematic error]) × 10^{-5} in the LISM. Because deuterium is converted by nuclear reactions in stars to ^{3}He and ^{4}He (a process usually called "astration") over the lifetime of the Galaxy, and this deuterium-depleted gas is returned to the interstellar medium (ISM) by stellar winds and supernova explosions, the D/H ratio in the LISM pro-

[1] Based on observations with the NASA/ESA *Hubble Space Telescope*, obtained at the Space Telescope Science Institute, which is operated by the Association of Universities for Research in Astronomy, Inc., under NASA contract NAS 5-26555.

[2] JILA, University of Colorado, Boulder, CO 80309-0440.

vides a lower limit to the cosmologically important primordial D/H ratio and also provides an important constraint on Galactic chemical evolution models. By studying the gas in the α Cen line of sight, we are testing whether the D/H ratio is essentially constant in the LISM, as implied by the short timescale for mixing of interstellar gas, or whether there are significant variations in the D/H ratio, as suggested by *Copernicus* observations (see, e.g., Dupree, Baliunas, & Shipman 1977; Bruston et al. 1981).

The high spectral resolution ($\lambda/\Delta\lambda = 90{,}000$) and signal-to-noise (S/N) capabilities of the GHRS and the suppression of geocoronal Lyman-α emission achievable with the use of the 0".25 × 0".25 Small Science Aperture (SSA) make the GHRS a far superior instrument than *Copernicus* or the *International Ultraviolet Explorer* (*IUE*) for studies of D/H and the dynamics of the LISM. The GHRS has been used so far to study a number of lines of sight through the LISM including as targets Capella, Procyon, G191−B2B (Lemoine et al. 1995), Sirius (Lallement et al. 1994), α PsA (Ferlet et al. 1995), Altair, Vega, β Pic, δ Cas (Lallement et al. 1995), and ϵ CMa (Gry et al. 1995).

Analyses of these lines of sight have led to the following picture of the LISM as summarized by Lallement et al. (1995). The Sun lies near the edge of what is called the local interstellar cloud (LIC), which is also called the AG cloud because it is centered in the anti-Galactic center direction. This cloud appears to move as a rigid body because high-resolution spectra of nearly all nearby stars show significant interstellar absorption at velocities within 1 km s^{-1} of the projected velocity of the LIC flow vector. In addition, most stars show additional absorption features centered at other velocities, which is usually interpreted as evidence of other clouds that presumably lie outside the LIC. The gas temperature and nonthermal motions (often called turbulence) in the LIC can be derived from the line widths of ions that differ greatly in atomic mass. The resonance lines of D I, Fe II, and Mg II are quite suitable for this purpose. The Capella and Procyon lines of sight (see Paper II) have provided perhaps the most accurate values for these parameters, $T = 7000 \pm 500$ (and ± 400 systematic error) K and $\xi = 1.20 \pm 0.27$ km s^{-1}, where ξ is the most probable speed for the assumed Gaussian nonthermal motions. Frisch (1995) provides a comprehensive review of the physical and dynamic properties of the LISM.

The α Cen line of sight provides a critical test of this picture because it is the only star studied so far by the GHRS that lies in the general direction of the Galactic center, and the interstellar Fe II and Mg II absorptions for this line of sight have velocities inconsistent with the LIC flow vector (Lallement et al. 1995). In fact, Lallement & Bertin (1992) placed α Cen in a different cloud, their so-called G (for Galactic) cloud, with a slightly different flow vector. Analysis of the α Cen spectra may, therefore, provide answers to the questions of where the LIC ends and the G cloud begins in this direction, the physical properties of the G cloud, and whether D/H in the G cloud differs from that in the LIC. The GHRS has measured D/H so far only for gas in the LIC. Most stars studied to date with the GHRS probably lie outside the LIC, and thus the derived H I column densities provide only a lower limit to the H I number density in the LIC. On the other hand, the line of sight to α Cen likely lies entirely or mostly within the G cloud, so that one can determine the H I number density in the G cloud from the H I column density.

When analyzing lines of sight with low H I column densities, one should consider whether hydrogen in the heliosphere contributes significantly to the total hydrogen absorption. The interaction between the ionized solar wind and the partially ionized interstellar gas flowing toward the Sun is now thought to create three discontinuities in the flow: a bow shock located at 200–500 AU in the upwind direction, the heliopause separating the flow of interstellar plasma from that of the solar-wind plasma, and the solar-wind termination shock located at about 100–200 AU in the upwind direction where the solar wind makes the transition from supersonic to subsonic flow (cf. Baranov & Malama 1995). The neutral component of the interstellar gas flows through the solar system, but charge exchange with solar-wind protons slows and heats this flow, forming a region of enhanced neutral-hydrogen density called the "hydrogen wall" located between the bow shock and the heliopause at roughly 200 AU in the upwind direction. We believe that we have detected the hydrogen wall through redshifted absorption by the heated hydrogen in the α Cen line of sight, and for the first time we can estimate its column density and temperature (see § 4.5).

The determination of D/H in the LISM involves the measurement of the neutral-deuterium column density ($N_{\rm D\,I}$) and the neutral-hydrogen column density ($N_{\rm H\,I}$) by interstellar absorption in the hydrogen and deuterium Lyman-α lines against the stellar chromospheric Lyman-α emission line. Since the D I Lyman-α line is optically thin toward α Cen and relatively narrow, we can interpolate the stellar emission line background to obtain an accurate value of $N_{\rm D\,I}$. On the other hand, the H I Lyman-α absorption feature is very broad and saturated, so we must model the unknown stellar emission line. Errors in its assumed line shape can translate into large systematic errors in the derived value of $N_{\rm H\,I}$. Thus, the main uncertainty in D/H is the H I column rather than the D I column. For this reason, we pay very careful attention to the roles played by the uncertain stellar emission line and the influence of heliospheric hydrogen. This care required a great many simulations to characterize the random and systematic errors to be placed on the derived parameters. In this paper, we consider parameter errors to be random when they characterize the quality of the fit to the data and errors in the derived parameters to be systematic when they are a consequence of the unknown emission-line profile background.

The GHRS spectra are described in § 2, and we present in § 3 our determination of the interstellar parameters and D/H ratio under several different assumptions. In § 4, we compare our derived interstellar parameters with those obtained for other lines of sight, and we also discuss models of H I in the heliosphere and how they relate to our analysis.

2. GODDARD HIGH RESOLUTION SPECTROGRAPH OBSERVATIONS OF ALPHA CENTAURI

We observed α Cen A on 1995 May 1 and α Cen B on 1995 May 5 by using the echelle gratings of the GHRS and the SSA to obtain the highest possible spectral resolution and to suppress the geocoronal Lyman-α emission. For a description of the GHRS instrument, see Brandt et al. (1994) and Heap et al. (1995). Soderblom et al. (1994) describe the improved characteristics of the GHRS with COSTAR when α Cen was observed. Table 1 summarizes the observations, including the spectral resolutions and integration times. The echelle data were obtained in the FP-SPLIT mode to

TABLE 1

SUMMARY OF GODDARD HIGH RESOLUTION SPECTROGRAPH OBSERVATIONS

Grating	Aperture and Substep Pattern	Spectral Range (Å)	Spectral Resolution (km s^{-1})	Exposure Time (s)	Start Time (UT)	Important Features
			α Cen A (1995 May 1)			
G140L.....	LSA 5	1200–1490	360	186	14:47	H I 1216 Å
EA–46.....	SSA 9	1212–1219	3.57	2786	15:02	H I + D I 1216 Å
EB–20.....	SSA 7	2792–2806	3.54	485	17:40	Mg II 2796, 2803 Å
EB–22.....	SSA 7	2593–2605	3.27	646	17:52	Fe II 2599 Å
			α Cen B (1995 May 5)			
EB–20.....	SSA 7	2792–2806	3.54	700	10:25	Mg II 2796, 2803 Å
EA–46.....	SSA 9	1212–1219	3.57	3231	12:04	H I + D I 1216 Å

reduce fixed-pattern noise and were processed with the version of the CALHRS software available in 1995 May. The individual readouts of the FP-SPLIT spectra were combined by using a cross-correlation procedure called HRS_MERGE (Robinson et al. 1992). Images of the platinum calibration lamp were taken prior to all observations and used to calibrate the wavelengths of the spectra.

We observed the Mg II *h* and *k* resonance lines (at 2803 Å and 2796 Å) in both stars and the Fe II multiplet UV1 (at 2599 Å) in α Cen A only. Our objective in observing lines of these elements, which have much larger atomic weights than H or D and therefore have narrower absorption lines, was to search for multiple velocity components in this line of sight and to measure the thermal and turbulent broadening independently. Figure 1 shows the complete echelle B spectra. The high resolution of the Ech-B grating separates the very narrow and deep interstellar Mg II and Fe II lines from the broader stellar chromospheric Mg II emission lines and photospheric Fe II absorption line (see § 3.1).

Our spectra of the Mg II *h* and Fe II lines of α Cen A are essentially identical in shape to the GHRS spectra obtained in 1992 by Lallement et al. (1995), except that our fluxes are lower (by factors of 5.6 and 4.8 for the Mg II and Fe II spectra, respectively), presumably because of the star's being misplaced at the edge of the small aperture. Comparison with Mg II fluxes measured by *IUE* (see, e.g., Cerruti-Sola, Cheng, & Pallavicini 1992) confirms that the fluxes of the 1992 observations are correct, so we have normalized the fluxes of our spectra to agree with those of the 1992 spectra. (Fig. 1 and all subsequent figures show the corrected fluxes.) Acquisition and precise centering in the 0.″25 × 0.″25 SSA for the α Cen stars are difficult because of the rapid motion of these stars, the brightness of each star, and the proximity of the bright companion star (about 18″ away). Our wavelength calibrations are accurate because our α Cen A and α Cen B spectra and the 1992 α Cen A spectra show the same ISM velocities for the Fe II and Mg II lines.

Figure 2 shows the spectra of the Lyman-α region of both stars. Superposed on the broad Lyman-α emission lines formed in the chromospheres of the stars are broad saturated absorption features (centered at 1215.6 Å) due to interstellar H I and narrower absorption lines due to interstellar D I, predicted to lie at −0.3307 Å (corresponding to −81.6 km s^{-1}) relative to H I. The flux of the Lyman-α line of α

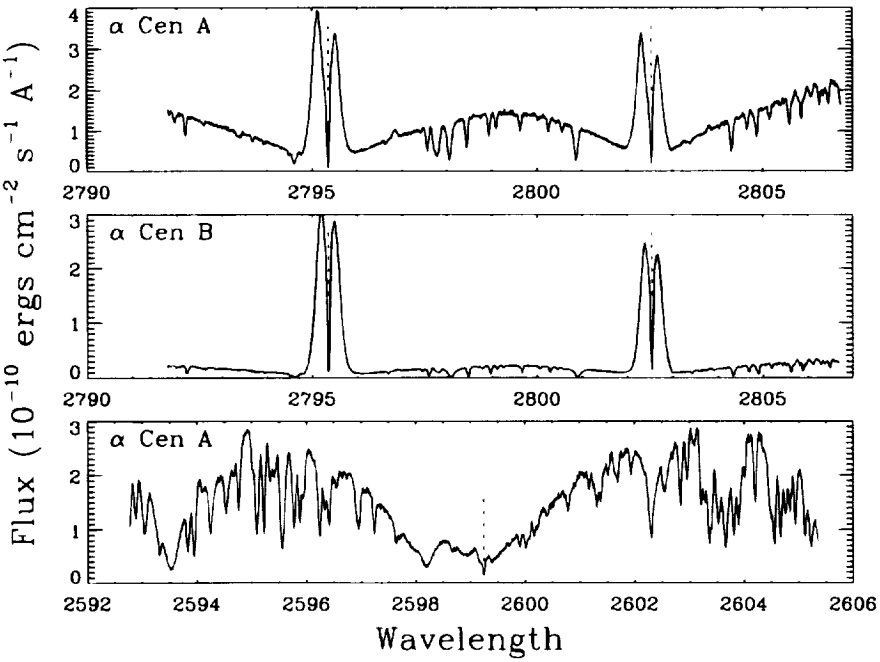

FIG. 1.—Our echelle-B observations of the Mg II *h* and *k* lines (at 2802.7 and 2795.5 Å) for α Cen A and α Cen B (*upper two panels*) and the Fe II 2599.4 Å line of α Cen A (*bottom panel*). The dotted lines mark the locations of interstellar absorption lines.

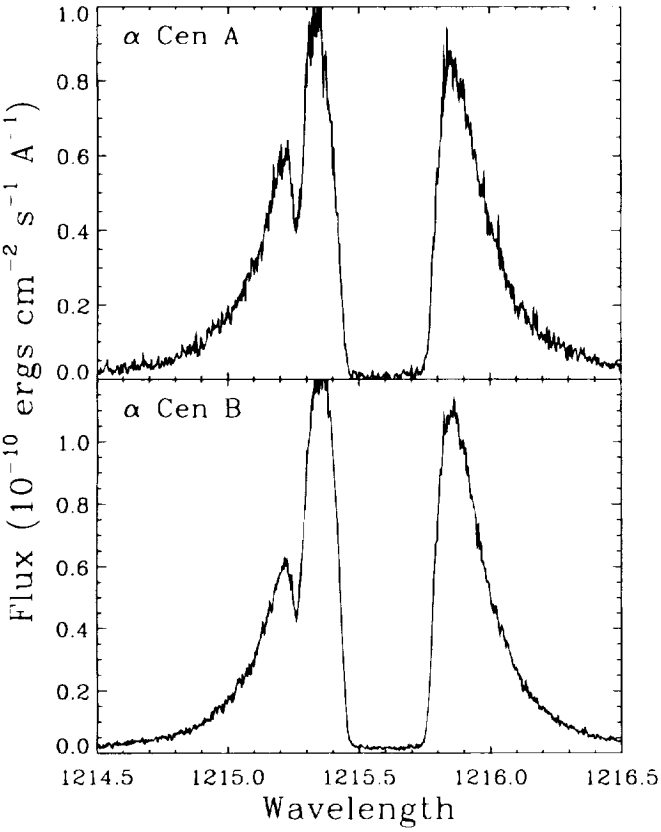

FIG. 2.—Our echelle-A observations of the Lyman-α lines of α Cen A and α Cen B, showing broad interstellar H I absorption centered at 1215.6 Å and narrow D I absorption near 1215.25 Å.

Cen A was a factor of 3.3 times lower than that observed during the G140L observation listed in Table 1. This confirms that α Cen A was not well centered in the SSA during our high-resolution observations. Since the G140L spectrum was taken through the Large Science Aperture (LSA) rather than the SSA, the flux calibration should be much more reliable. Therefore, we increased the fluxes of our Lyman-α spectrum of α Cen A by a factor of 3.3 to obtain consistency with the G140L data. Since the velocity of the interstellar D I line is consistent with the velocities of the Fe II and Mg II lines, we believe the wavelength calibration is accurate.

Owing to a guide star acquisition failure, the α Cen B observations were obtained in coarse track guiding mode on a single guide star, meaning the accuracy of the centering of the star in the aperture is highly suspect for these observations. The first science observation after acquisition was the Mg II observation. We find that the Mg II fluxes we observed are consistent with those observed by the *IUE* (see, e.g., Cerruti-Sola et al. 1992). We also find that the velocities of the interstellar Mg II absorption lines are the same as those seen in the α Cen A spectra, which means that the wavelength calibration of this spectrum is accurate. Because the fluxes and wavelengths appear to be correct, α Cen B was apparently well centered in the SSA at the beginning of our observations. However, during the subsequent observation of the Lyman-α line we believe the star must have been slowly drifting out of the aperture because inspection of the 16 individual readouts of this FP-SPLIT observation shows that the count rates decreased throughout the observation. We therefore use the first readout of the observation to flux-calibrate the spectrum. This procedure amounts to multiplying the fluxes of the combined spectrum by a factor of 1.3. We also find that the velocity of the interstellar D I line is redshifted by 0.9 km s^{-1} with respect to the interstellar D I absorption line observed for α Cen A (which has a velocity consistent with the velocities measured for Fe II and Mg II). This discrepancy is also probably due to the star's drifting out of the aperture during the observation, and so we have changed the wavelengths by 0.9 km s^{-1} to make this observation consistent with the others. (Note that Fig. 2 and all subsequent figures show the corrected fluxes and wavelengths for the Lyman-α lines of α Cen A and α Cen B.)

The D I lines in Figure 2 are well separated from the interstellar H I absorption, and since they are not very deep they must be optically thin. On the other hand, the interstellar H I lines are very saturated with sharp core boundaries, indicating that these lines lie on the flat part of the curve of growth with H I column densities log $N_{\rm H\,I} \sim 18$. Thus, the absorption line shape depends both on the H I column and the broadening parameter $b_{\rm H\,I}$. The saturated H I absorption core has positive flux, which can result only from scattered light in the GHRS spectrograph. This problem has been seen previously in our Lyman-α spectra of Capella (Paper I). In our analysis and in all figures except Figure 2, we correct for this scattered light by simply subtracting the mean flux level in the saturated core (9.9×10^{-13} erg cm^{-2} s^{-1} Å^{-1} and 1.9×10^{-12} erg cm^{-2} s^{-1} Å^{-1} for α Cen A and α Cen B, respectively) from the fluxes observed between 1215.35 and 1215.85 Å.

3. PROPERTIES OF THE LINE OF SIGHT TO ALPHA CENTAURI

3.1. *Single-Component Fits to the Line Profiles*

We first analyze each line profile of each star separately without imposing any constraints on the derived parameters, except to minimize the χ^2 of the fit. It is important, however, to estimate as accurately as feasible the intrinsic stellar emission or absorption line upon which the interstellar absorption is superposed, as uncertainties in the assumed stellar line profile can be the dominant source of error, especially for the highly saturated H I line.

Figure 3 shows our fit to the α Cen A stellar and interstellar Fe II 2599 Å lines, for both our data and the higher S/N archival data. Figures 4 and 5 show our fits to the Mg II *h* and *k* lines for both stars and, for the α Cen A *h* line, both data sets. The thin solid lines in the figures represent our best guesses for the intrinsic stellar line profiles, estimated by using polynomial fits to the spectral regions blueward and redward of the interstellar absorption lines. The thick solid lines, which fit the observations very well, are the convolution of the computed interstellar absorption lines (*dotted lines*) and the instrumental point-spread function, which is approximated as a Gaussian with FWHM = 3.7 pixels (Gilliland 1994). There is no evidence for any asymmetry in the absorption lines, and the residuals of our one-component fits (shown below each spectrum) reveal no dependence on velocity that would suggest the presence of a second component.

The parameters for these fits are listed in Table 2 together with random errors estimated by using Monte Carlo simulations. We have matched the observed profiles very well, but the derived ISM parameters for the two Mg II lines and

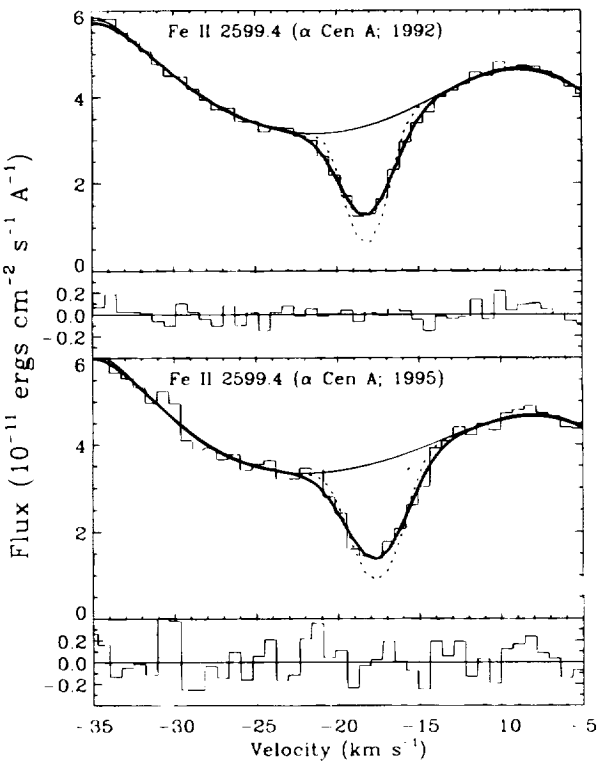

FIG. 3.—Our best fits to the Fe II interstellar absorption lines observed toward α Cen A in 1992 and in 1995. The parameters of the fits are given in Table 2. The data are shown in histogram form. The thin solid lines are our estimates for the stellar emission above the absorption lines, computed by using polynomial fits to spectral regions blueward and redward of the absorption. The dotted line is the best-fit absorption line before convolution with the instrumental profile, and the thick solid line is this absorption line after instrumental broadening. The residuals are plotted below each fit.

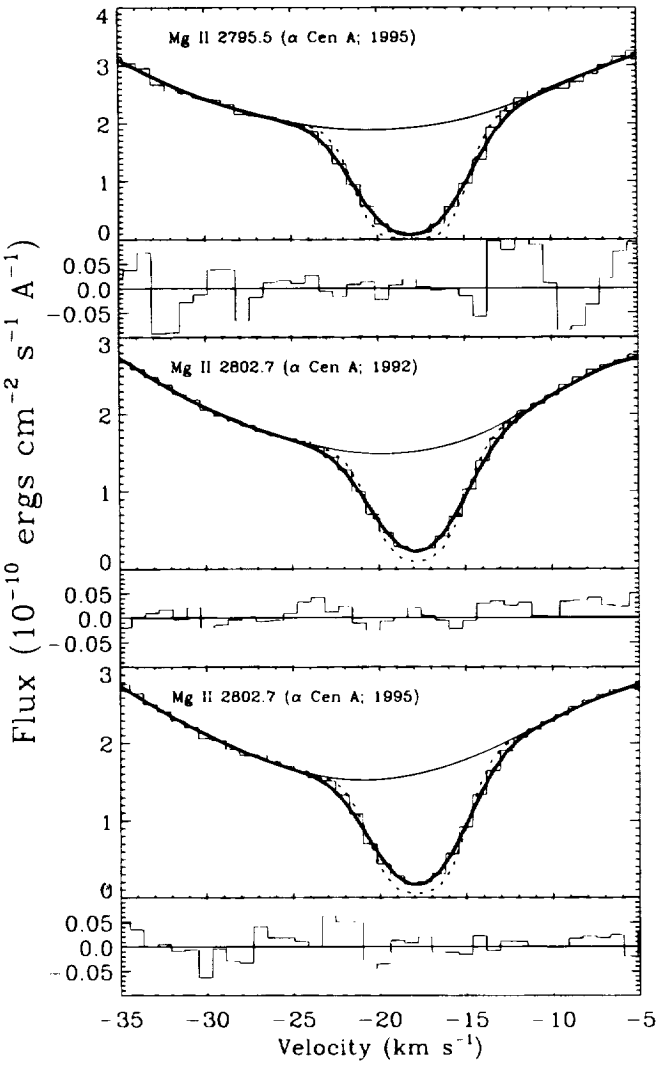

FIG. 4.—Our best fits to the Mg II interstellar absorption lines observed toward α Cen A in 1992 and in 1995. The parameters of the fits are given in Table 2. The various lines that are displayed have the same meaning as in Fig. 3.

for the same lines in the two stars often lie outside each other's formal statistical errors. This is probably due to the systematic uncertainties in our estimates of the intrinsic stellar line profiles in the vicinity of the interstellar features. The $b_{\mathrm{Fe\ II}}$-values for the two data sets differ from each other by a little more than 2 σ, but the Fe II lines have widths very close to the instrumental resolution, making it difficult to infer an accurate value for $b_{\mathrm{Fe\ II}}$, especially for the noisier 1995 data. The heliocentric velocities listed in Table 2 are consistent with the predicted -18.1 km s^{-1} velocity of the local interstellar flow for the Galactic center direction proposed by Lallement & Bertin (1992).

In Figure 6, we fit the interstellar D I absorption lines by using polynomial fits to estimate the "continua" against which the D I absorption lines are measured. Each of these continua actually represents the combination of the stellar emission line plus some absorption in the wings of the inter-

TABLE 2

INTERSTELLAR PARAMETERS FOR THE SINGLE-COMPONENT FITS

Star	Ion	Line	Velocity (km s^{-1})	b (km s^{-1})	log N	τ	χ^2
α Cen A[a].....	Fe II	2599.396	-18.2 ± 0.1	1.43 ± 0.02	12.441 ± 0.004	1.64	0.701
α Cen A	Fe II	2599.396	-17.7 ± 0.1	1.78 ± 0.14	12.455 ± 0.022	1.39	1.641
α Cen A	Mg II	2795.528	-18.1 ± 0.1	2.32 ± 0.04	12.698 ± 0.017	5.50	1.708
α Cen A[a].....	Mg II	2802.705	-17.8 ± 0.1	2.26 ± 0.02	12.691 ± 0.003	2.76	5.000
α Cen A	Mg II	2802.705	-17.8 ± 0.1	2.21 ± 0.04	12.776 ± 0.010	3.35	1.624
α Cen B.....	Mg II	2795.528	-18.2 ± 0.1	2.49 ± 0.01	12.640 ± 0.003	4.48	5.349
α Cen B.....	Mg II	2802.705	-18.0 ± 0.1	2.19 ± 0.01	12.802 ± 0.003	3.61	4.924
α Cen A	D I	1215.339	-18.2 ± 0.1	6.55 ± 0.27	12.799 ± 0.015	0.72	0.928
α Cen B.....	D I	1215.339	-18.2 ± 0.1	6.88 ± 0.17	12.775 ± 0.009	0.65	1.334
α Cen A	H I	1215.670	-15.9 ± 0.1	11.80 ± 0.05	18.031 ± 0.003	68671	1.090
α Cen B.....	H I	1215.670	-15.6 ± 0.1	11.81 ± 0.02	18.027 ± 0.002	68111	2.211

[a] Spectra obtained by Lallement et al. 1995.

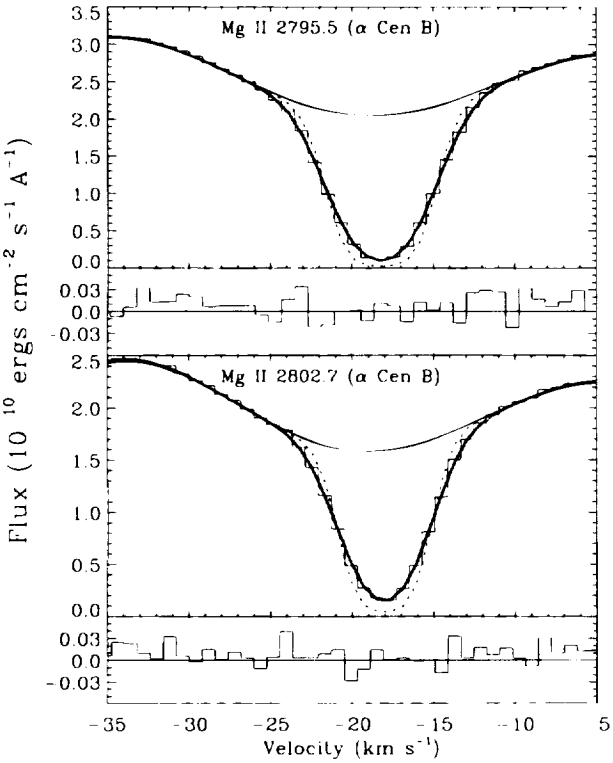

FIG. 5.—Our best fits to the Mg II interstellar absorption lines observed toward α Cen B in 1995. The parameters of the fits are given in Table 2. The various lines that are displayed have the same meaning as in Fig. 3.

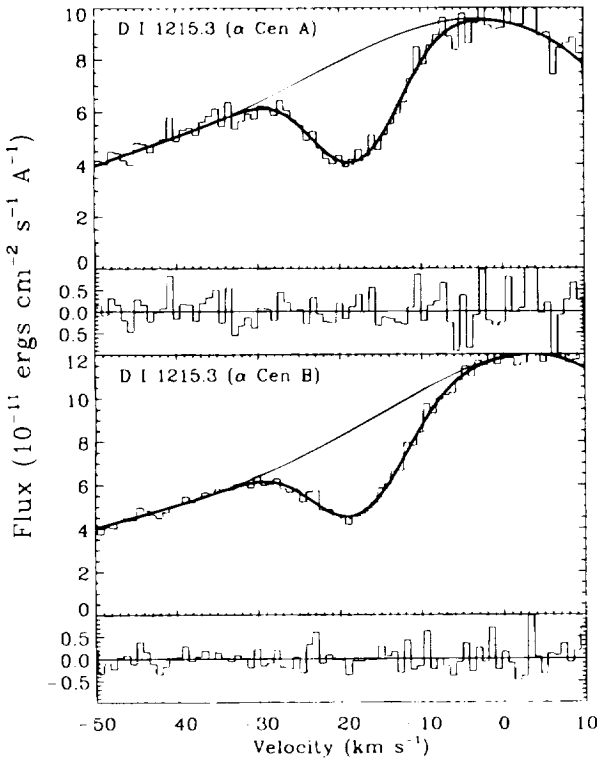

FIG. 6.—Our best fits to the D I interstellar absorption lines observed toward α Cen A and α Cen B. The parameters of the fits are given in Table 2. The various lines that are displayed have the same meaning as in Fig. 3. The dotted lines showing the best-fit profile before instrumental smoothing are barely distinguishable from the thick solid lines.

stellar H I absorption profile. For Capella and Procyon it was not possible to fit D I separately from H I (see Papers I and II), as we have done here, because for each of those two cases the widths of the Lyman-α emission line and the interstellar H I absorption line act to create a local flux maximum somewhere in the spectral region of the D I line. This local flux maximum makes it very difficult to estimate the "continuum" for the D I absorption line by looking only at that spectral region. For α Cen A and α Cen B, though, we believe that we can accurately extrapolate a continuum above the D I absorption lines without determining the shape of the stellar Lyman-α profile and then correcting for the interstellar H I absorption. For all of our fits to the D I and H I lines, we have included both components of the fine structure doublet, which has a velocity spacing of 1.33 km s^{-1}.

In fitting the H I line profiles, we initially ignore the D I lines by using the same polynomial interpolation scheme used for the D I fits to remove the interstellar D I absorption. The process we use to construct the intrinsic stellar Lyman-α profiles is described below and illustrated in Figure 7. Because both α Cen A and α Cen B are solar-like main-sequence stars, we use the quiet-Sun profile from Brekke et al. (1991) as the starting point of our analysis (*dotted lines in the figure*). However, α Cen A and α Cen B

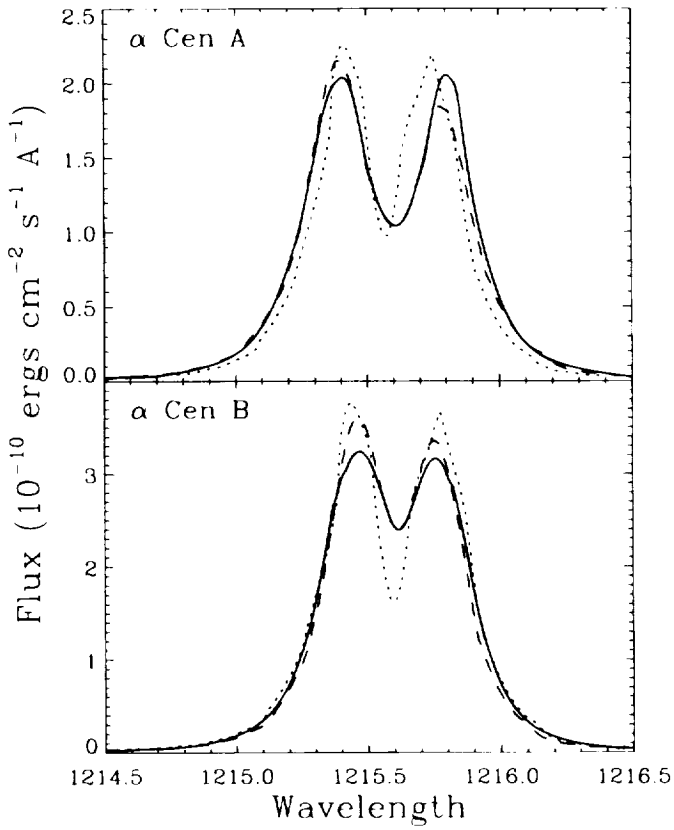

FIG. 7.—An illustration of how we estimated the intrinsic stellar Lyman-α profiles of α Cen A and α Cen B (see text for details). The dotted line is the quiet-Sun Lyman-α profile taken from Brekke et al. (1991). The dashed lines are our initial guesses for the stellar Lyman-α profiles. For α Cen A (α Cen B), the wings of the dashed line are based on broadening (narrowing) the solar Lyman-α profile by 10% (6%). The centers of the dashed lines are based on the Mg II *k* lines observed for α Cen A and α Cen B. The assumed stellar profiles were altered to improve the quality of single-component fits to the interstellar H I absorption lines, and the solid lines show the stellar profiles after these alterations.

have luminosities different from the Sun's, and the widths of optically thick chromospheric lines such as Lyman-α are dependent on the stellar luminosity, with the higher luminosity stars having the broader lines. This phenomenon, which is called the Wilson-Bappu effect (Wilson & Bappu 1957), was first studied using the Ca II H and K lines, but a similar correlation exists for the Mg II *h* and *k* lines (see, e.g., Vladilo et al. 1987) and the Lyman-α line (Landsman & Simon 1993). We have compared the Mg II *k* line profile of the Sun with those of α Cen A and α Cen B, and we find that the α Cen A line is roughly 10% broader than the solar line and the α Cen B line is roughly 6% narrower. This result is consistent with the Wilson-Bappu effect, since α Cen A is somewhat more luminous and α Cen B is less luminous than the Sun. Assuming that the widths of Lyman-α scale like those of Mg II, we next broaden (narrow) the solar Lyman-α line by 10% (6%) and scale the resulting profile to agree with the far wings of the α Cen A (α Cen B) line. This procedure provides our initial estimates for the wings and sides of the Lyman-α lines.

The shapes of the centers of the Lyman-α profiles are estimated from the observed Mg II *k* lines, because for the Sun and Procyon (see Paper II) we have found that the Mg II *k* and Lyman-α lines have very nearly the same shape when plotted on a $\Delta\lambda$ scale (as opposed to a velocity scale). This similarity in shape can be understood in terms of both lines being optically thick chromospheric lines with self-reversals. We therefore use the observed α Cen A and α Cen B Mg II *k* line profiles to estimate the shapes of the cores of the stellar Lyman-α lines, which we combine with the line wings estimated from the scaled solar Lyman-α profiles. The dashed lines in Figure 7 show the resulting profiles, which represent our initial guesses for the α Cen A and α Cen B Lyman-α profiles. Our initial fits to the data using these profiles were not very good, so we used the residuals of those first fits to alter the assumed profiles slightly and then we refit the data. We went through this procedure one more time before converging on the profiles shown as solid lines in Figure 7. The best fits to the data assuming these profiles are shown in Figure 8, and the parameters of the fits are given in Table 2. We note that the Lyman-α fluxes of the stellar Lyman-α profiles shown in Figures 7 and 8 are very similar to those that would be observed from the Sun at the distance of α Cen. The intrinsic central reversals are located entirely within the saturated interstellar absorption and thus play no role in the derived interstellar parameters.

The fits displayed in Figure 8 match the data well, although the residuals reveal systematic discrepancies seen for both stars (near 1215.42 Å and 1215.75 Å) that cannot be removed by any reasonable alteration of the assumed stellar Lyman-α lines. Note that the computed Lyman-α line fits both the steep sides of the absorption core, which depend on both $N_{\rm H\,I}$ and $b_{\rm H\,I}$, and the far wings of the line beyond the emission peaks, which depend only on $N_{\rm H\,I}$. It is very encouraging that the parameters of our single-component fits to the α Cen A and α Cen B data are almost identical (see Table 2). This is strong evidence that extracting information on the ISM from the observed H I absorption lines is a well-posed problem with a unique solution—at least for single-component fits.

The line width parameter $b = (0.0165T/A + \xi^2)^{1/2}$ km s^{-1}, where A is the atomic weight and ξ is the most probable speed (in km s^{-1}) of the assumed Gaussian turbulent motions. The combination of the *b*-values for D ($A = 2$), Mg ($A = 24.3$), and Fe ($A = 55.8$) allows us to solve for T and ξ separately. The shaded region of Figure 9 shows the allowed range of these parameters given the values and uncertainties of $b_{\rm D\,I}$, $b_{\rm Mg\,II}$, and $b_{\rm Fe\,II}$ for the two stars. From Figure 9, we quote values of $T = 5400 \pm 500$ K and $\xi = 1.20 \pm 0.25$ km s^{-1} for the temperature and nonthermal velocity, respectively, for the α Cen line of sight.

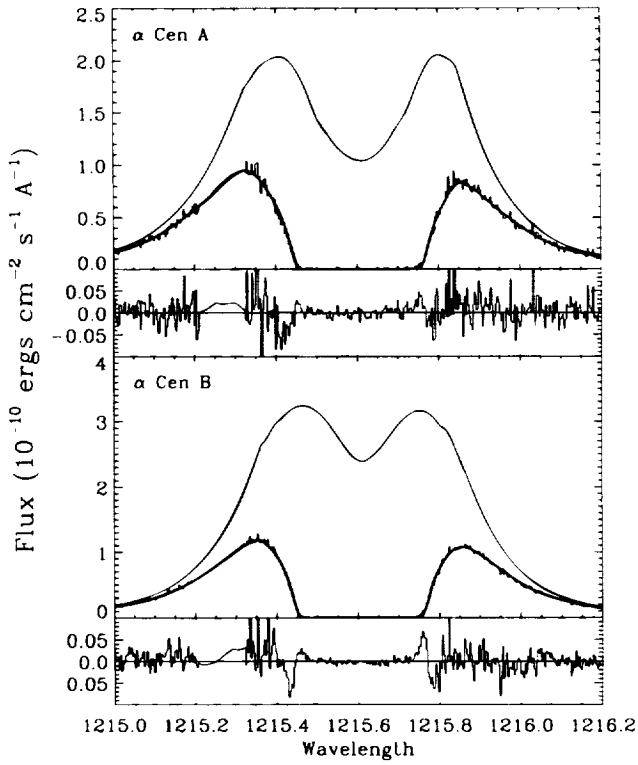

FIG. 8.—Our best single-component fits to the H I absorption lines of α Cen A and α Cen B. The parameters of the fits are given in Table 2. The data are shown in histogram form, where the D I absorption at 1215.25 Å has been removed by using polynomial fits. The thin solid lines are our best estimates of the intrinsic stellar line profiles (see text and Fig. 7). The thick solid lines are the fits to the data, and the residuals are shown below each fit. The difference between the computed absorption lines before and after smoothing with the instrumental profile is too small to be visible on these plots.

There are three surprising results from our one-component analysis of the α Cen ISM absorption lines that concern us and will be addressed in the next sections, where we explore models with multiple components and different intrinsic stellar emission line profiles.

1. The ISM velocities measured by the fits to the Fe II, Mg II, and D I lines are nearly identical and collectively imply $v = -18.0 \pm 0.2$ for the α Cen line of sight, but the centroid of the H I absorption is shifted by about +2.2 km s^{-1} for both α Cen A and α Cen B. One expects, perhaps naively, that hydrogen and deuterium should be well mixed in the ISM and share the same flow velocities within measurement errors. However, Landsman et al. (1984) had previously called attention to a similar discrepancy in their analysis of less accurate *Copernicus* and *IUE* spectra. They found that for α Cen A, the D I line is blueshifted by 8 ± 2 km s^{-1} relative to H I (or H I is redshifted by the same amount relative to D I).

2. Second, the value of $b_{\rm H\,I}$ and the temperature it implies are larger than the values inferred from the other line widths

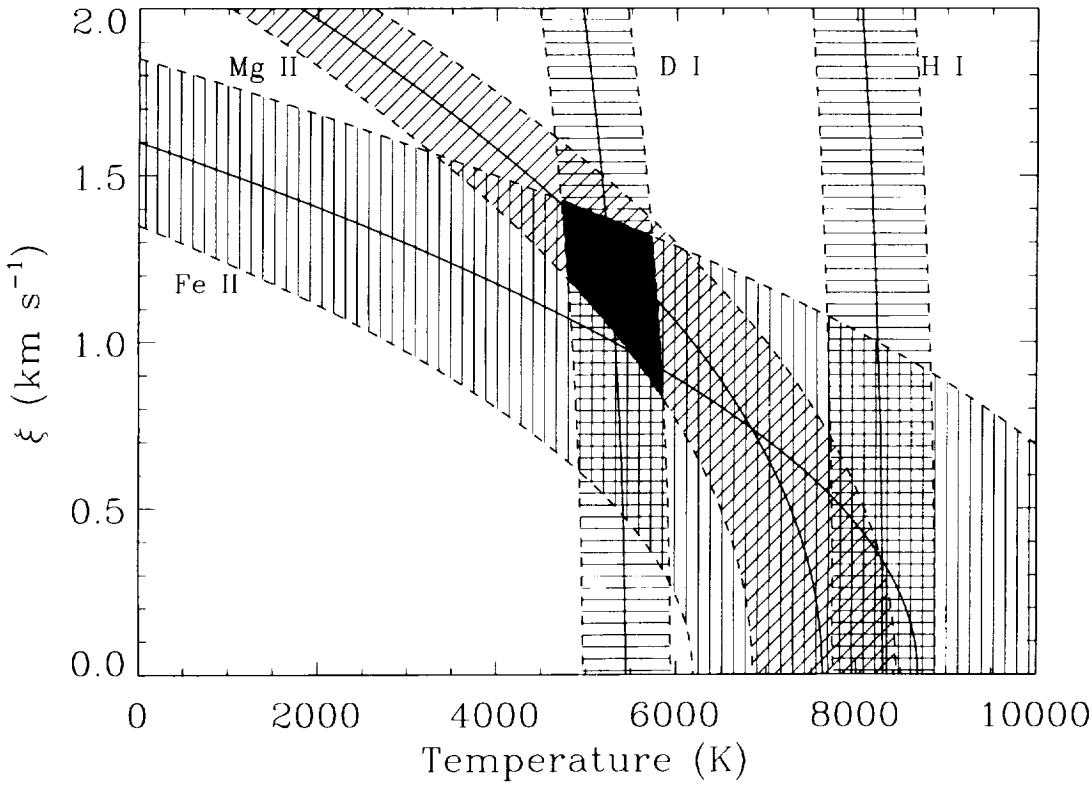

FIG. 9.—Combination of the *b*-values given in Table 2 for D I, Mg II, and Fe II allows us to solve for the temperature of the interstellar medium, T, and the nonthermal velocities present in the ISM, ξ. The allowable ranges of T and ξ are shown for D I, Mg II, and Fe II separately, and the shaded region shows where these regions overlap. Also shown are the obviously discrepant allowable ranges of T and ξ suggested by the single-component fits to H I (see § 3.1).

(see Fig. 9). By using the values $T = 5400$ K and $\xi = 1.2$ km s^{-1} derived from the D I, Mg II, and Fe II lines, we compute $b_{\rm H\,I} = 9.51$ km s^{-1}, which is 2.3 km s^{-1} smaller than observed. An alternative way of looking at this result is to assume the measured values for $b_{\rm H\,I}$ and $\xi = 1.20$ km s^{-1} to obtain $T = 8350$ K, almost 3000 K hotter than inferred from the other lines. Landsman et al. (1984, 1986), in their analysis of the *Copernicus* and *IUE* spectra, had also called attention to the very broad hydrogen profiles for these stars with $b_{\rm H\,I} > 11$ km s^{-1} for α Cen A and $b_{\rm H\,I} > 13.8$ km s^{-1} for α Cen B.

3. From the fits in Figures 6 and 8, we find that the D/H ratio is $(5.86 \pm 0.24) \times 10^{-6}$ for the α Cen A data and $(5.60 \pm 0.14) \times 10^{-6}$ for α Cen B. These D/H ratios are consistent within their cited errors and together imply a value of D/H = $(5.7 \pm 0.2) \times 10^{-6}$. This result is very different from the D/H = 1.6×10^{-5} value found for the Capella and Procyon lines of sight.

Are these results real or spurious, perhaps produced by inaccurate intrinsic Lyman-α profiles and/or by the assumption that the gas along this short line of sight is homogeneous?

If true, the D/H = $(5.7 \pm 0.2) \times 10^{-6}$ result could have profound implications for both cosmology and our understanding of the LISM because this is a very different result from that found in Papers I and II (D/H = 1.6×10^{-5}). It is important, therefore, to determine whether our α Cen data are really inconsistent with D/H = 1.6×10^{-5}. Since D I is optically thin, log $N_{\rm D\,I}$ should be well determined, and so decreasing log $N_{\rm H\,I}$ is the only possibility. For D/H to be 1.6×10^{-5}, log $N_{\rm H\,I}$ must be decreased to 17.6. In Figure 10 we have fit the Lyman-α lines again, but this time we have forced log $N_{\rm H\,I}$ to be 17.6. For these fits we have altered the assumed stellar profiles from those used in Figure 8 to ones that produce better fits for low values of $N_{\rm H\,I}$. This approach amounts to decreasing the fluxes and broadening the profiles a bit. Despite these changes, Figure 10 shows that single-component fits with log $N_{\rm H\,I} = 17.6$ are incapable of fitting the data. The sides of the observed absorption lines are simply not steep enough.

It seems sensible that hydrogen and deuterium should be well mixed and therefore share the same flow velocity and have line broadening parameters consistent with the same values of T and ξ. We therefore fit the H I and D I absorption lines toward each star while imposing the constraint that the velocities and broadening parameters of H and D are consistent with the D I fits in Figure 6. The results are shown in Figure 11. The fits are again very poor. The H I absorption of the models are clearly blueshifted relative to the data, and the saturated cores of the model absorption profiles are clearly too narrow. Thus, for single-component models, the velocity and temperature of hydrogen cannot be forced to be consistent with the velocity and temperature of deuterium.

3.2. *Two-Component Fits to the Line Profiles*

A second H I absorption component is obviously required to make the velocity and temperature of H I consistent with D I, Fe II, and Mg II. This second component must have a H I column density high enough to modify the observed H I absorption significantly, but not high enough to produce observable D I, Fe II, or Mg II absorption. We first considered whether geocoronal H I absorption could be responsible. At the time of these observations, the Earth

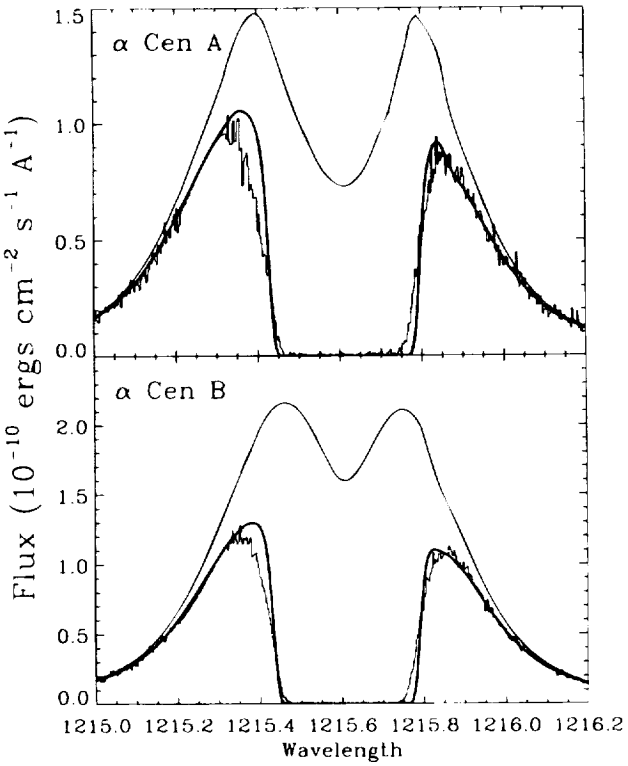

FIG. 10.—Fits to the H I absorption lines of α Cen A and α Cen B, in which the H I column density has been forced to be $10^{17.6}$. The assumed stellar profiles (*thin solid lines*) have been altered from those used in Fig. 8 to ones that maximize the quality of fits with log $N_{\rm H\,I} = 17.6$, but the fits (*thick solid lines*) are very poor despite this change. This result proves that for single-component fits, log $N_{\rm H\,I}$ cannot be 17.6 and thus, D/H cannot be consistent with the D/H-value obtained for the Capella and Procyon lines of sight (Paper II).

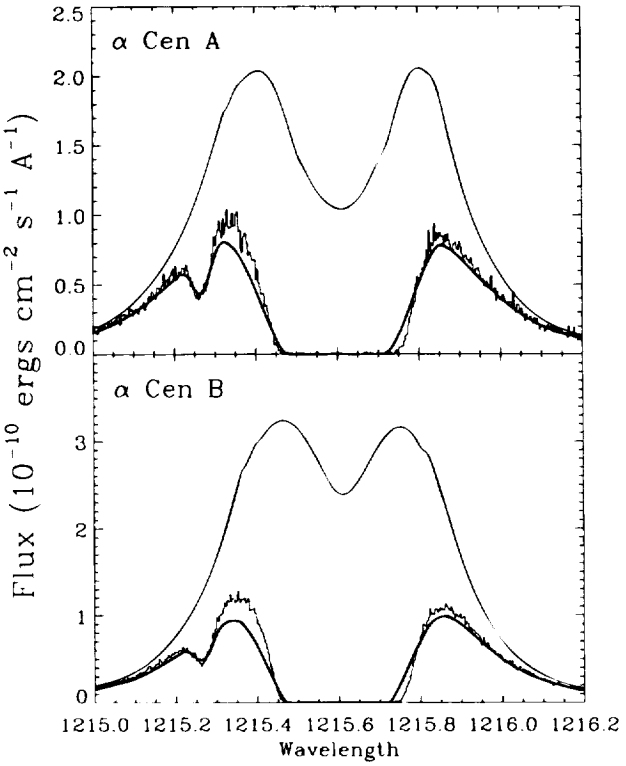

FIG. 11.—Fits to the H I and D I absorption lines of α Cen A and α Cen B in which the velocities and Doppler parameters of the lines are forced to be consistent with the velocities, temperatures, and nonthermal velocities measured from the D I fits in Fig. 6. The poor quality of the fits demonstrates that for a single-component fit, the velocity and temperature of H I cannot be consistent with those values for D I.

was moving toward α Cen A at +7.3 km s^{-1} and toward α Cen B at +5.9 km s^{-1} in the heliocentric reference frame. Absorption by H I at these velocities could in principle produce the observed H I redshift, but these velocities are still well within the saturated core of the H I absorption. We find that for temperatures reasonable for geocoronal H I ($T \approx 1000$ K), H I column densities of about 10^{17} cm^{-2} are necessary to broaden the absorption in the manner that we require. This column density is much too high, as typical H I column densities in the geocorona are 10^{13} cm^{-2}. (According to the thermal exosphere model of Heiden (1988), typical values at 400 km are $T = 1035$ K and $n_{\rm H\,I} = 1 \times 10^5$ cm^{-3}.)

Because the H I Lyman-α line is on the flat portion of the curve of growth, the addition of a small amount of hot H I in the line of sight will broaden the line core, and displacing this hot hydrogen component by a few km s^{-1} from the main component could explain the net redshift of the H I line relative to the D I line and the larger than expected value of $b_{\rm H\,I}$. Thus, when we fit the D I and H I absorption lines simultaneously with two components and force consistency between D I and H I, the second component invariably ends up being hot and redshifted. These fits are shown in Figure 12, and the fitted parameters are given in Table 3. The assumed stellar profiles have been altered slightly from those used in Figure 8 to maximize the quality of the two-component fits. Since it is difficult to measure accurately the parameters of highly blended components such as those in Figure 12, we forced the velocities and Doppler parameters of the components representing the bulk of the ISM absorption (dotted lines in the figure) to be consistent with the D I fits in Figure 6. Therefore, no errors are given for these parameters in Table 3. For the fits in Figure 12, we forced the D/H ratio to be the same for both components, but D I

TABLE 3

INTERSTELLAR PARAMETERS FOR THE TWO-COMPONENT FITS TO LYMAN-α

Star	Profile Model	Velocity (km s^{-1})	$b_{\rm H\,I}$ (km s^{-1})	log $N_{\rm H\,I}$	D/H (10^{-5})	τ	χ^2
α Cen A.....	1A	−18.2	9.3	18.014 ± 0.005	0.59 ± 0.03	83766	1.002
		−14.4 ± 0.2	20.01 ± 0.67	15.088 ± 0.101	0.59 ± 0.03	46.31	1.002
α Cen B.....	1B	−18.2	9.7	17.991 ± 0.003	0.62 ± 0.02	75841	1.589
		−13.8 ± 0.1	22.17 ± 0.27	14.860 ± 0.028	0.62 ± 0.02	24.77	1.589
α Cen A.....	2A	−18.2	9.3	17.658 ± 0.014	1.28 ± 0.10	36887	1.105
		−15.7 ± 0.2	24.86 ± 0.46	14.843 ± 0.034	1.28 ± 0.10	21.21	1.105
α Cen B.....	2B	−18.2	9.7	17.597 ± 0.007	1.54 ± 0.05	30631	1.436
		−15.3 ± 0.1	23.03 ± 0.18	15.007 ± 0.017	1.54 ± 0.05	33.39	1.436

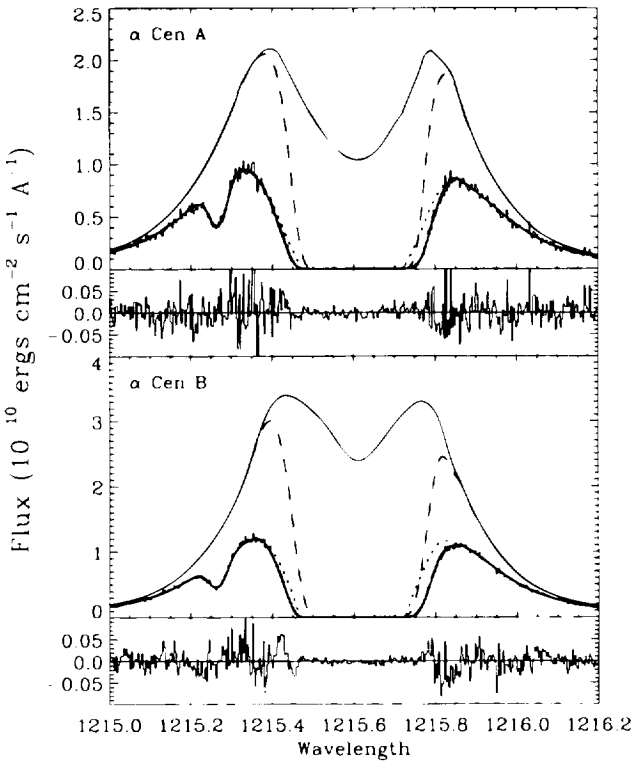

FIG. 12.—Two-component fits to the H I and D I absorption lines of α Cen A and α Cen B. The parameters of these fits are given in Table 3. The assumed stellar Lyman-α profiles (*thin solid lines*) are nearly the same as those used in Fig. 8, although they have been altered slightly to improve the quality of the fits. The dotted lines show the component representing the bulk of the interstellar medium. For both the α Cen A and α Cen B fits, the velocity and Doppler parameter of this component has been forced to be consistent with the velocity and temperature of the ISM implied by the D I fits in Fig. 6. The dashed lines show a hot component that we believe represents absorption from hot H I near the heliopause (see § 4.5). The thick solid lines show the combination of the two absorption components, and the residuals of the fits are shown below each fit.

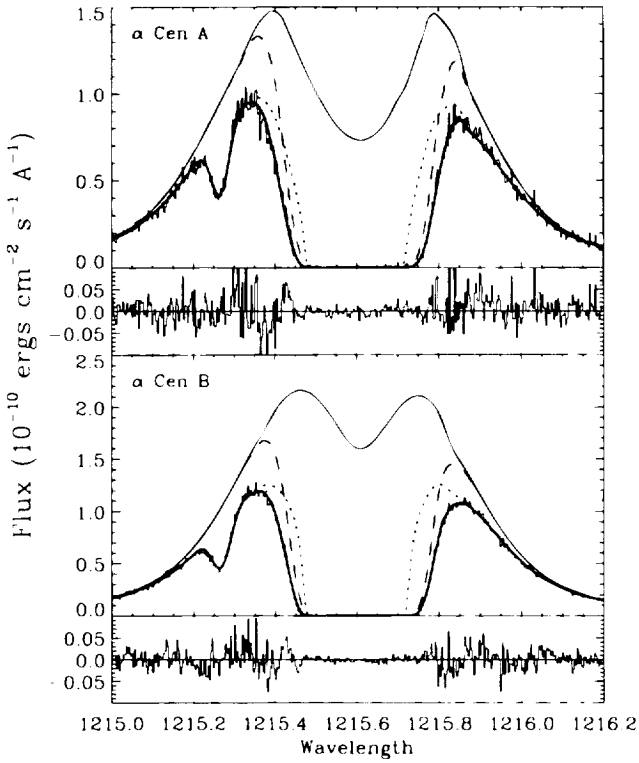

FIG. 13.—Same as Fig. 12, but using different stellar emission profiles. For these fits, the derived interstellar H I column density is much lower than for the fits in Fig. 12 (see Table 3).

absorption is completely negligible for the hot component (dashed lines in the figure) because the hot H I column density is so low. According to the fits, the second component has a Doppler parameter characteristic of temperatures of about 27,000 K and is redshifted by about 4 km s^{-1} relative to the main component. We believe that this second component is due to interstellar H I that has flowed into the heliosphere and is compressed and heated near the heliopause by interaction with the solar wind. The column density, redshift, and temperature of our second component are consistent with recent models of the outer heliosphere, which predict the existence of this "hydrogen wall." These models will be discussed further in § 4.5.

We now consider whether the addition of a second component changes our conclusions about the D/H ratio for the α Cen line of sight. The D/H-values implied by the two-component fits in Figure 12 are not much different from the results of the single-component fits. This similarity is not surprising, considering that the stellar profiles are nearly the same as those in Figure 8. The question is this: Can we find an acceptable fit to the data with a completely different D/H-value by altering the assumed profiles? The answer was "no" for single-component fits (see Fig. 10). However, in Figure 13 we use the same stellar profiles that were used in Figure 10, and we find that acceptable two-component fits do exist when using those profiles. On the basis of the fit parameters given in Table 3, the D/H-values for the fits in Figure 13 are much higher than the D/H = $(5.7 \pm 0.2) \times 10^{-6}$ value we obtained from the single-component fits. We have no direct way of determining whether the intrinsic profiles in Figure 12 (hereafter profiles 1A and 1B) or Figure 13 (profiles 2A and 2B) are better representatives of the stellar Lyman-α emission lines, and so we must consider both as plausible options. *Thus, we find that the existence of the second component destroys our ability to measure precise values of D/H from our data.*

3.3. *Three-Component Fits to the Line Profiles*

The two-component fits in Figures 12 and 13 are certainly improvements over the single-component fits in Figure 8, as demonstrated by both the residuals and the χ^2-values. Nevertheless, there is at least one remaining systematic discrepancy between the models and the data. All the fits in Figures 12 and 13 show a narrow flux excess near 1215.42 Å, which could be explained by temperature gradient in the ISM or temperature gradients in the heliospheric interface region (HIR), but we have represented the ISM and hydrogen wall with single-temperature components. Another problem with the two-component models is that the α Cen line of sight passes not only through the Sun's heliosphere, but also through an analogous "astrosphere" of α Cen. (Since the prefix "helio-" implies a connection with the Sun, we replace the "helio-" prefix with "astro-.") In other words, there should be two hydrogen walls along this line of sight, and it is important to determine how the existence of a second hydrogen wall may affect our analysis.

According to Lallement & Bertin (1992), the interstellar flow vector for the solar neighborhood is directed toward

$\ell = 186.^{\circ}1$ and $b = -16.^{\circ}4$ with a velocity of $v_0 = 25.7$ km s^{-1}. The α Cen line of sight is at an angle of $\theta = 52^{\circ}$ with respect to the upwind direction of this vector. In order to determine what the interstellar flow looks like in the rest frame of α Cen, we assume that the V_G vector of Lallement & Bertin (1992) is appropriate (see also Lallement et al. 1995), and we assume a distance, proper motion, and radial velocity for α Cen of $d = 1.34$ pc, $\mu_\alpha = -3.''640$ yr^{-1}, $\mu_\delta = +0.''700$ yr^{-1}, and $v = -22.0$ km s^{-1} (Hirshfeld, Sinnott, & Ochsenbein 1991). On the basis of these quantities and α Cen's position of $\alpha(2000) = 14^h39^m36^s$ and $\delta(2000) = -60^{\circ}50'10''$, we find that the ISM flow vector for α Cen is ($\ell = 286.^{\circ}8$, $b = -78.^{\circ}7$, $v_0 = 22.6$ km s^{-1}) and the line of sight toward the Sun is at an angle of $\theta = 79^{\circ}$ with respect to the upwind direction.

The α Cen values for v_0 and θ (22.6 km s^{-1}, 79°) are not too different from the solar values (25.7 km s^{-1}, 52°). We also note that the stellar winds of α Cen A and α Cen B are probably similar to the solar wind, as α Cen A and α Cen B are both relatively inactive, main-sequence, solar-like stars. Thus, we conclude that the properties of α Cen's astrospheric interface region (AIR) along the Sun–α Cen line of sight are probably not that different from the properties of the solar HIR for this line of sight. Note that α Cen A and α Cen B probably share the same astrosphere, since the stars are only about 46 AU apart (Heintz 1982), and the solar example suggests distances of about 200 AU from the stars to the "astropause" (the stellar equivalent of the heliopause).

The ISM flow velocity for the α Cen line of sight is -18.0 km s^{-1}, and the stellar radial velocity for α Cen is -22.0 km s^{-1}. Models of the solar hydrogen wall (see, e.g., Baranov & Malama 1995) suggest that the velocity of α Cen's hydrogen wall should be somewhere between -18.0 km s^{-1} and -22.0 km s^{-1} because the material in the wall should be decelerated relative to the star. Thus, the α Cen AIR absorption should produce either a slight blueshift of the H I absorption line relative to the D I, Mg II, and Fe II lines, or no observable shift, since the velocity separation between the ISM absorption and the α Cen AIR absorption is small. However, we observe a significant redshift for H I, not a small blueshift. In contrast, the solar HIR absorption should lie somewhere between 0 and -18 km s^{-1} and can therefore produce a H I absorption line that is significantly redshifted relative to D I, Mg II, and Fe II, in agreement with our observations. Therefore, the hot components of Figures 12 and 13 should definitely be attributed to the HIR rather than the AIR of α Cen. However, the fit parameters for this second component may be inaccurate because we have neglected the possible contributions of α Cen's AIR to the H I absorption.

We have performed three-component fits to the data to see how the addition of the third component (representing α Cen's AIR) affects the parameters derived for the second component (representing the solar HIR). The results using profile models 1A and 1B are shown in Figure 14, and Figure 15 shows the fits obtained assuming profiles 2A and 2B. The parameters for all these fits are given in Table 4. It is very difficult, if not impossible, to separate absorption components as highly blended as the three components in Figures 14 and 15. To reduce the number of free parameters,

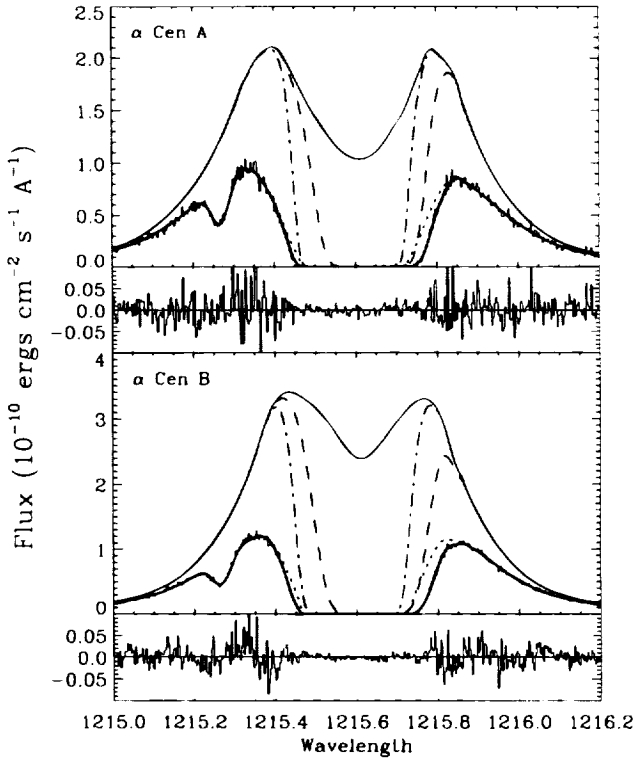

FIG. 14.—Same as Fig. 12, but with the addition of a third component (*dash-dotted lines*) that is meant to represent absorption by hot hydrogen in the neighborhood of α Cen, analogous to the absorption near the Sun represented by the second component. The parameters of these fits are given in Table 4.

TABLE 4

INTERSTELLAR PARAMETERS FOR THE THREE-COMPONENT FITS TO LYMAN-α

Star	Profile Model	Velocity (km s^{-1})	b_{HI} (km s^{-1})	log N_{HI}	D/H (10^{-5})	τ	χ^2
α Cen A.....	1A	−18.2	9.3	18.016 ± 0.004	0.58 ± 0.03	84131	0.965
		−8.0	19.30 ± 0.60	14.633 ± 0.070	0.58 ± 0.03	16.83	0.965
		−20.0	15.01 ± 1.14	15.555 ± 0.335	0.58 ± 0.03	180.6	0.965
α Cen B.....	1B	−18.2	9.7	17.997 ± 0.002	0.60 ± 0.02	76816	1.389
		−8.0	21.35 ± 0.23	14.513 ± 0.020	0.60 ± 0.02	11.55	1.389
		−20.0	16.06 ± 0.48	15.171 ± 0.101	0.60 ± 0.02	67.46	1.389
α Cen A.....	2A	−18.2	9.3	17.654 ± 0.014	1.29 ± 0.08	36549	1.096
		−8.0	22.39 ± 0.56	14.439 ± 0.045	1.29 ± 0.08	9.29	1.096
		−20.0	24.83 ± 0.55	14.575 ± 0.034	1.29 ± 0.08	11.47	1.096
α Cen B.....	2B	−18.2	9.7	17.603 ± 0.007	1.52 ± 0.06	31028	1.406
		−8.0	22.00 ± 0.27	14.542 ± 0.020	1.52 ± 0.06	11.98	1.406
		−20.0	21.29 ± 0.26	14.831 ± 0.026	1.52 ± 0.06	24.09	1.406

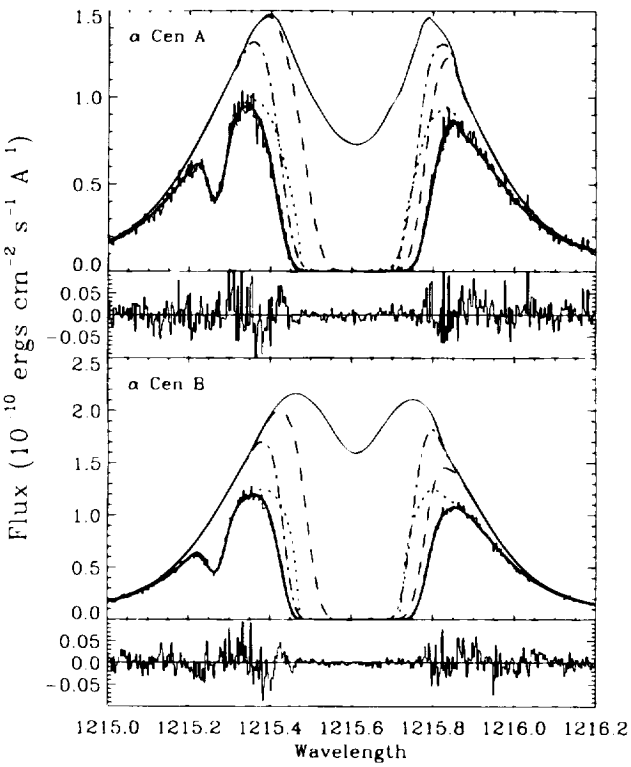

FIG. 15.—Same as Fig. 14, but using different stellar emission profiles. The assumed Lyman-α profiles are the same as those used in Fig. 13.

we forced the velocity and Doppler parameter of the ISM component (*dotted lines*) to be consistent with the parameters of the D I fits in Figure 6, as we did for the two-component fits. We also fixed the velocities of the HIR and AIR components to be -8 km s^{-1} and -20 km s^{-1}, respectively. These velocities are consistent with the theoretical predictions of Baranov & Malama (1995).

The derived parameters of the third component, representing α Cen's AIR, are $\log N_{\rm H\,I}^{(3)} = 15.03 \pm 0.43$ and $b_{\rm H\,I}^{(3)} = 19.5 \pm 4.6$ km s^{-1}, respectively. These parameters varied quite a bit among the four fits listed in Table 4, which explains the large errors. The column density and Doppler parameter of the third component are similar to the values we find for the second component of the two- and three-component fits, consistent with our prediction that α Cen's AIR should be similar to the HIR of the Sun.

For the two-component fits, we found that the parameters of the hot component representing the HIR are $\log N_{\rm H\,I}^{(2)} = 14.95 \pm 0.11$, $b_{\rm H\,I}^{(2)} = 22.5 \pm 2.0$ km s^{-1}, and $v_{\rm H\,I}^{(2)} = -14.8 \pm 1.2$ km s^{-1}. We now compare these parameters with the parameters of the second component of the three-component fits in order to obtain our best estimates for the solar hydrogen wall parameters. Because we found it necessary to fix the velocities of the HIR and AIR components in Figures 14 and 15, we can only give a lower limit of $v_{\rm H\,I}^{(2)} > -16$ km s^{-1} for the velocity of the solar hydrogen wall. The addition of the third component slightly lowered the derived Doppler parameter of the HIR component from $b_{\rm H\,I}^{(2)} = 22.5 \pm 2.0$ km s^{-1} to $b_{\rm H\,I}^{(2)} = 21.3 \pm 1.4$ km s^{-1}, and lowered the column density from $\log N_{\rm H\,I}^{(2)} = 14.95 \pm 0.11$ to $\log N_{\rm H\,I}^{(2)} = 14.53 \pm 0.08$. By averaging the results of all 8 two- and three-component fits, we find that our best estimates and 1 σ errors for the parameters of the HIR are $v_{\rm H\,I}^{(2)} > -16$ km s^{-1}, $b_{\rm H\,I}^{(2)} = 21.9 \pm 1.7$ km s^{-1} (corresponding to a temperature of $T = 29{,}000 \pm 5000$ K), and $\log N_{\rm H\,I}^{(2)} = 14.74 \pm 0.24$.

4. DISCUSSION

4.1. *The* H I *Column Density to* α *Cen*

We have found that the H I column density toward α Cen is determined mainly by fitting the shape of the observed Lyman-α line wings and thus depends critically upon the width of the wings of the assumed stellar emission line. On the other hand, the shape of the observed line cores provides information on the hot gas that we think is near the heliopause (see § 4.5) rather than in the interstellar medium. Thus, the values of $\log N_{\rm H\,I}$ and D/H depend upon whether profiles 1A and 1B or profiles 2A and 2B are better representations of the intrinsic stellar emission lines.

The wings of profiles 1A and 1B are based on the mean quiet-Sun profile obtained with the HRTS (High Resolution Telescope Spectrograph) experiment and kindly provided to us by P. Brekke (Brekke et al. 1991). To our knowledge there are no high-resolution Lyman-α profiles from the whole Sun viewed as a star. The wings of profiles 2A and 2B are roughly 10% broader than those of profiles 1A and 1B. Profiles 1A and 1B represent our "best guesses" for the intrinsic stellar profiles, but are the broader 2A and 2B profiles sensible alternatives? HRTS spectra of the Sun with high spatial resolution show relatively narrow profiles over most of the solar disk but much brighter profiles with broader wings over active regions (see, e.g., Basri et al. 1979). The fractional coverage of active regions on the Sun varies with the solar cycle, and the coverage of presumably analogous active regions on α Cen A and α Cen B is unknown. Active regions will broaden the Lyman-α profiles somewhat in spatially averaged stellar spectra. We expect that the Lyman-α profile for the Sun viewed as a star could have somewhat broader wings than the mean quiet-Sun profile used to construct profiles 1A and 1B and that the same should be true for the α Cen stars. Thus, profiles 2A and 2B are plausible representations of the intrinsic emission lines, and the interstellar hydrogen column density could be near $\log N_{\rm H\,I} = 17.6$ rather than 18.0 derived by using profiles 1A and 1B. Because the error in the hydrogen column is dominated by the uncertain width of the intrinsic emission line profile rather than the random errors in the data or the formal errors derived by the fitting program, we adopt $\log N_{\rm H\,I} = 17.8 \pm 0.3$ as a rough but generous allocation for this systematic error that includes both possible solutions.

Landsman et al. (1984, 1986) analyzed *IUE* Lyman-α spectra and reanalyzed archival *Copernicus* spectra of the α Cen stars. For α Cen A they obtained $\log N_{\rm H\,I} = 17.08$–$17.92$, and for α Cen B they found $\log N_{\rm H\,I} < 17.78$. These ranges for the hydrogen column are considerably larger than our findings, but they overlap the values we derive from GHRS spectra. Our derived range for the neutral-hydrogen column toward α Cen is also consistent with the value $N_{\rm H\,I} = 9 \times 10^{17}$ cm^{-2} that Mewe et al. (1995) found by modeling the *Extreme Ultraviolet Explorer* (*EUVE*) spectrum of α Cen. R. Mewe (1995, private communication) has stated that the uncertainty in their hydrogen column is $N_{\rm H\,I} = (9 \pm 1) \times 10^{17}$ cm^{-2}, which corresponds to $\log N_{\rm H\,I} = 17.95 \pm 0.05$. Finally, Quémerais et al. (1994) derived the H I density, $n_{\rm H\,I} = 0.165 \pm 0.035$ cm^{-3},

for the LISM gas flowing into the solar system from comparisons of radiative-transfer calculations with interplanetary and geocoronal diffuse Lyman-α emission. This result corresponds to a column density of log $N_{\rm H\,I} = 17.83 \pm 0.09$ toward α Cen, consistent with our results. Our value of log $N_{\rm H\,I} = 17.80 \pm 0.30$ corresponds to $n_{\rm H\,I} = 0.076$–0.30 cm^{-3} and D/H = (0.5–1.9) $\times 10^{-5}$. Our parameters are compared in Table 5 with those derived for the lines of sight to Procyon and Capella (Paper II).

4.2. *The Flow Velocity Along the α Cen Line of Sight*

We have found that the main velocity component along the line of sight toward α Cen (obtained from the D I, Mg II, and Fe II lines) has a bulk heliocentric flow speed of $v = -18.0 \pm 0.2$ km s^{-1}, which is consistent with the speed of -18.1 km s^{-1} predicted by the flow vector in the Galactic center direction ($V_{\rm G}$) proposed by Lallement & Bertin (1992). If we had used their anti-Galactic center vector ($V_{\rm AG}$), the projected velocity would have been -15.7 km s^{-1}. For Capella, Procyon, and many other stars, ISM absorption consistent with the $V_{\rm AG}$ vector is observed, but no absorption is seen that is at the velocity predicted by the $V_{\rm G}$ vector (see Papers I and II; Lallement et al. 1995). However, most or all of the line of sight toward α Cen appears to be through the $V_{\rm G}$ gas.

Which vector represents the true LISM flow vector for the solar neighborhood? Lallement et al. (1995) have argued that the Sun is located in gas that is flowing with the $V_{\rm AG}$ vector, partly because α Cen seems to be the exception rather than the rule and partly because the 26 ± 1 km s^{-1} velocity of interstellar He I atoms measured by *Ulysses* (Witte et al. 1993) agrees with the modulus of the $V_{\rm AG}$ vector rather than the faster velocity of 29 km s^{-1} predicted by the $V_{\rm G}$ vector. These arguments do not explain, however, why we see no evidence of any material toward α Cen moving at the velocity predicted by the $V_{\rm AG}$ vector. Assuming that the Sun does in fact lie in the AG cloud, Lallement et al. (1995) have estimated that the AG cloud can at most account for only about 2%–4% of the interstellar column density observed toward α Cen, and they have interpreted this small percentage to mean that the boundary between the AG and the G clouds (assuming they are in fact separate clouds) must be very nearby along the α Cen line of sight.

4.3. *The Temperature and Nonthermal Gas Motions Toward α Cen*

The mean temperature and turbulent velocity of the gas toward α Cen are $T = 5400 \pm 500$ K and $\xi = 1.20 \pm 0.25$ km s^{-1}, respectively. The nonthermal motions, which we have modeled as Gaussian microturbulence, are the same as for the Procyon ($\xi = 1.21 \pm 0.27$ km s^{-1}) line of sight and are consistent with the value ($\xi = 1.6 \pm 0.4$ km s^{-1}) derived for the Capella line of sight (see Paper II). We have no way of knowing whether these nonthermal motions are a consequence of unresolved discrete velocity components, rotation of the LIC, expansion of the cloud along the line of sight, or true turbulent motions. The motions are definitely subsonic, and we conclude that there is no shock front in the LIC near the Sun and thus no shock heating at this time.

On the other hand, the mean temperature of the interstellar gas toward α Cen is apparently lower than toward Capella ($T = 7000 \pm 500$ K) and Procyon ($T = 6900 \pm 300$ K), both of which lie either outside or near the edge of the LIC. Lallement et al. (1995) also noted that the interstellar Fe II and Mg II lines toward α Cen A are narrow, which suggests that the gas in this line of sight is probably cooler than the gas in the LIC, but they did not have profiles of the D I line to determine the temperature accurately. Our data provide the first conclusive evidence that the interior of the G cloud is cooler than the edge of the LIC, which can be heated more effectively by the external UV radiation field and thermal conduction from the presumably hotter surrounding gas.

The H I number density ($n_{\rm H\,I} = 0.076$–0.30 cm^{-2}) and temperature ($T = 5400 \pm 500$ K) of the interstellar gas toward α Cen correspond to a thermal pressure (including 10% helium) $P/k = 410$–1950 cm^{-3} K. We assume that this pressure is representative of the gas located toward the center of the G cloud. On the other hand, the Procyon and Capella data indicate a slightly higher temperature ($T = 7000$ K) when looking through the LIC in the outward direction. The density in the outward direction is not known, but if we assume $n_{\rm H\,I} = 0.076$–0.30 cm^{-2}, the thermal pressure $P/k = 580$–2310 cm^{-3} K.

Wolfire et al. (1995) have computed models of the ISM in ionization and thermal equilibrium. They have found that three stable phases are possible for a limited range of pres-

TABLE 5

COMPARISON OF INTERSTELLAR PARAMETERS

PARAMETER	α CEN A/B (Profile 1)	α CEN A/B (Profile 2)	CAPELLA (Linsky et al. 1995)	PROCYON (Linsky et al. 1995)
l	316°	316°	163°	214°
b	−1°	−1°	5°	13°
d (pc)	1.34	1.34	12.5	3.5
$v_{\rm main}$ (km s^{-1})	−18.0	−18.0	22.0 ± 0.9	20.8 ± 1.5
$v_{\rm LISM}$ (km s^{-1})	−18.1	−18.1	22.0	19.8
$v_{\rm other}$ (km s^{-1})	−14.1	−15.5	...	23.4 ± 1.5
T (K)	5400 ± 500	5400 ± 500	7000 ± 500	6900 ± 300
ξ (km s^{-1})	1.20 ± 0.25	1.20 ± 0.25	1.6 ± 0.4	1.21 ± 0.27
$N_{\rm H\,I}$ (10^{17} cm^{-2})	10.1	4.2	17.1–17.6	11.2–11.8
$\langle n_{\rm H\,I}\rangle$ (cm^{-3})	0.24	0.102	0.0443–0.0456	0.104–0.109
$d_{\rm edge}$ (pc)	...	...	1.9–7.3	1.2–4.8
D/H (10^{-5})	0.61	1.41	1.60 ± 0.09	1.6
log (Mg II/H I)	−5.28	−4.91	−5.41	−5.50
log (Fe II/H I)	−5.55	−5.18	−5.75	−5.76
D I/Mg II	1.2 ± 0.2	1.2 ± 0.2	4.1 ± 0.4	5.1 ± 0.7

sure: (1) a hot ionized medium (HIM) with $T \sim 10^6$ K, (2) a warm neutral medium (WNM) or warm ionized medium (WIM) with $T \sim 8000$ K, and (3) a cold neutral medium (CNM) with $T \sim 50$ K. The LIC is presumably in the WNM phase, in which heating is dominated by photoelectric heating of polycyclic aromatic hydrocarbons (PAHs) and cooling is dominated by radiation in the Lyman-α, C II (158 μm), and O I (63 μm) lines, and recombination to positive ions. If $P/k < 990$ cm^{-3} K, the HIM and WNM are stable, but the CNM is not stable, and there is no evidence for the CNM phase in the LIC. For their assumed standard conditions of the incident far ultraviolet radiation field and abundances and for $N_{\rm H\,I} = 10^{18}$ cm^{-2}, their equilibrium model has $T = 9200$ K when $n_{\rm H\,I} = 0.15$ cm^{-3}. For equilibrium conditions and $n_{\rm H\,I} = 0.10$ cm^{-3}, significantly lower pressures and temperatures are possible for lower values of the dust/gas (D/G) ratio; $P/k = 580$ cm^{-3} K corresponds to D/G $\approx$0.2 of the nominal values cited in their paper. WNM temperatures are very insensitive to abundances and the FUV radiation field when $n_{\rm H\,I} = 0.10$ cm^{-3}. Alternatively, the LIC may not be in ionization and thermal equilibrium. At present we cannot say which is the correct explanation for the low temperature and pressure in the LIC.

4.4. *Gas-Phase Abundances of* Fe *and* Mg *for the α Cen Line of Sight*

We now estimate the abundances of Fe and Mg in the α Cen line of sight by making the same assumptions as in Papers I and II. For the column densities of Fe II and Mg II we average the values for α Cen A and α Cen B: log $N_{\rm Fe\,II} = 12.45$ and log $N_{\rm Mg\,II} = 12.72$. For log $N_{\rm H\,I}$ we have adopted 17.80 ± 0.30. Therefore, log $(N_{\rm Fe\,II}/N_{\rm H\,I}) = -5.05$ to -5.65 and log $(N_{\rm Mg\,II}/N_{\rm H\,I}) = -4.78$ to -5.38.

Comparing these numbers to the solar abundances of Fe and Mg, log $({\rm Fe/H})_\odot = -4.49$ and log $({\rm Mg/H})_\odot = -4.41$ (Anders & Grevesse 1989), and assuming that the contributions to Fe II and Mg II from ionized gas are negligible, we derive the logarithmic depletions, $D({\rm Fe}) = (N_{\rm Fe\,II}/N_{\rm H\,I}) - \log({\rm Fe/H})_\odot = -0.56$ to -1.16 and $D({\rm Mg}) = (N_{\rm Mg\,II}/N_{\rm H\,I}) - \log({\rm Mg/H})_\odot = -0.37$ to -0.97 in the warm gas toward α Cen. It appears that Fe and Mg are less depleted toward α Cen than they are toward Capella [$D({\rm Fe}) = -1.28$ and $D({\rm Mg}) = -1.03$; Paper I] and Procyon [$D({\rm Fe}) = -1.27$ and $D({\rm Mg}) = -1.09$; Paper II].

The α Cen Mg and Fe depletion values can be compared to *Copernicus* estimates of $D_{\rm w}({\rm Mg}) = -0.3$ and $D_{\rm w}({\rm Fe}) = -1.4$ in the warm interstellar medium (Jenkins, Savage, & Spitzer 1986). The depletion for Fe is smaller than our α Cen measurement, and the value for Mg is somewhat larger. Most of the difference for Mg may be due to a systematic error in the *f*-values for the far-ultraviolet Mg II lines near 1240 Å used in the *Copernicus* study. Sofia, Cardelli, & Savage (1994) found that the far-UV lines of Mg II yield Mg II column densities 0.67 dex larger than those obtained from an analysis of the very strong but damped Mg II lines near 2800 Å. Because the *f*-values of the Mg II 2800 Å lines are well determined, Sofia et al. (1994) recommended a 0.67 dex revision to the *f*-values for the Mg II far-UV doublet. Although there may be difficulty with the Mg II result, the measurements for Fe II clearly reveal that substantial gas-phase depletion occurs in the cloud toward α Cen. Evidently the Fe in the cloud is found mostly in interstellar dust.

Because of the difficulty in measuring the column density of H I, the D/H ratio and the depletions of Mg and Fe are highly uncertain. Therefore, we are unable to determine whether D/H varies in the LISM, but we do find that the Mg and Fe depletions are at least slightly lower than those found toward Capella and Procyon. The D I/Mg II ratios, which are independent of the uncertain hydrogen column, are shown in Table 5 for α Cen, Capella, and Procyon. We find that D I/Mg II is nearly a factor of 4 smaller for the α Cen line of sight than for the Capella and Procyon lines of sight. *Thus, our data conclusively demonstrate that ISM abundances do vary significantly over distance scales of only a few parsecs, although we are not certain whether it is* D I *or* Mg II/Fe II *that is actually varying.* Because the Mg II and Fe II depletions in the interstellar medium are known to be variable (Jenkins 1987), the Mg II and Fe II ions seem to be the most likely culprits. This argument favors the use of Lyman-α profiles 2A and 2B rather than profiles 1A and 1B, because the fits with the former profiles suggest hydrogen columns consistent with variable Mg II and Fe II depletions and constant D/H in the LISM.

4.5. *A New Test of Gasdynamical Models of the Interstellar Gas and Solar Wind Interaction: Evidence for Compressed, Heated Interstellar Neutral Hydrogen*

For the past 25 years a succession of space instruments have studied the diffuse Lyman-α emission produced when H I atoms in the heliosphere (the region of space dominated by the solar wind) resonantly scatter solar Lyman-α photons. For example, Quémerais et al. (1994) inferred a value for the interplanetary H I density far from the Sun, $n_{\rm H\,I} = 0.165 \pm 0.035$ cm^{-3}, by analyzing Lyman-α absorption cell count rates obtained with the Atmospheric Lyman Alpha Experiment flown on the Space Shuttle in 1992. Their paper also provides a summary of the earlier observations of diffuse Lyman-α emission.

High-resolution spectra of the diffuse Lyman-α emission obtained with the GHRS and earlier instruments provide two critical facts concerning the properties of the H I atoms in the heliosphere. First, the heliocentric inflow speed is 20–21 km s^{-1} (first measured by Adams & Frisch 1977) rather than the 26 km s^{-1} velocity that characterizes both the LIC gas beyond the heliosphere and the neutral He inside the heliosphere (Lallement & Bertaux 1990; Lallement, Bertaux, & Clarke 1993; Clarke et al. 1995). The direction of the H I flow in the heliosphere and in the LIC are nearly identical (Lallement & Bertin 1992). Thus, H I is decelerated somewhere in the heliosphere by 5–6 km s^{-1} relative to the flow in the LIC. Second, the profile of the diffuse emission in both the upwind (the direction from which the interstellar gas appears to flow) and downwind directions can be fitted by a 30,000 K Voigt profile rather than the $\approx$7000 K temperature generally thought to characterize the interstellar gas, which implies that the H I is either heated or that the interplanetary flow pattern is complex (Clarke et al. 1995).

These spectroscopic data have stimulated the computation of self-consistent multifluid gasdynamical models of the interaction between the inflowing interstellar gas and the expanding solar wind. These models include charge-exchange collisions in which interstellar H I atoms exchange an electron with solar wind protons, forming secondary H I atoms. Without charge exchange, the primary H I atoms from the interstellar medium would penetrate unimpeded through the solar system, as previously thought, except for photoionization and radiation pressure within 30 AU. The

original models of Baranov & Malama (1993), which were for only one set of interstellar parameters ($n_{H\,I} = 0.14$ cm^{-3}, $n_p = 0.07$ cm^{-3}), have now been extended by Baranov & Malama (1995), Williams et al. (1996), and Zank et al. (1996) to include a range of interstellar parameters.

These new gasdynamical models typically show three discontinuities in the gas flow. The outermost discontinuity is a bow shock located at 200–500 AU from the Sun (depending on n_p in the ISM) in the upwind direction, where the flow of the ionized (plasma) component of the interstellar gas changes direction. The innermost discontinuity is the termination shock located at 100–200 AU, where the solar wind changes from a supersonic to a subsonic flow. Between these two shocks is the heliopause, the contact surface that separates the flow of interstellar plasma from that of the solar wind plasma. The location of these discontinuities depends critically on the uncertain fractional ionization of the interstellar medium; higher ionization leads to the boundaries lying closer to the Sun. In earlier heliospheric models the inflowing H I does not see these shocks, but rather flows through the expanding solar wind without collisions until about 30 AU from the Sun where photoionization and radiation pressure produce a cavity of neutral H I. In such models, beyond 30 AU from the Sun the density of H I is nearly constant and equal to the interstellar density, and the H I flow speed is also the same as the interstellar flow.

The main difference between the new and old models is the inclusion of charge-exchange collisions between the inflowing H I and the expanding solar wind protons, which then become secondary H I atoms with different momenta than the primaries. In these models, interactions between the primary and secondary H I atoms compress, decelerate, and heat the inflowing H I near the heliopause. This pile-up region of compressed H I in the upwind direction (first shown by Baranov, Lebedev, & Malama 1991) is now called the "hydrogen wall." In the models of Baranov & Malama (1995), the temperature of the hydrogen wall gas is about 20,000 K, whereas the models of Williams et al. (1996) indicate that 35,000 K is a typical upwind temperature for this gas all of the way into the inner solar system. Typical column densities for this warm H I are 10^{15} cm^{-2} both for typical LIC pressures and when the pressure is artificially raised by a factor of 3.5 to eliminate the bow shock. This higher pressure simulates the uncertain extra pressure terms from interstellar magnetic fields and cosmic rays. In the hydrogen wall the flow decelerates from the interstellar value of 26 km s^{-1} to 7–23 km s^{-1} depending on the assumed degree of ionization of the interstellar gas—higher ionization leads to more deceleration and forces the wall closer to the Sun. These models also predict 10^6 K (hot) H I primarily in the downwind direction. Charge exchange is unimportant for He I, so the He I atoms throughout the heliosphere retain the density and flow vector of the LIC.

Although recent models of the solar wind and interstellar medium interaction are rather sophisticated, more realistic extensions of this theoretical work are needed and would benefit from clear observational constraints on the important parameters. Quémerais et al. (1995) searched for an increase in the diffuse Lyman-α emission in the upwind direction that would be a signature of the hydrogen wall in their analysis of low-dispersion spectra from the *Voyager 1* and *Voyager 2* spacecraft, which were then 54 and 40 AU from the Sun. They indeed found an increase in the diffuse Lyman-α emission in the upwind direction, but they were unable to conclusively determine whether this increase was due to an enhancement of the H I density predicted by the models or to Galactic diffuse Lyman-α emission. GHRS Lyman-α spectra for the line of sight toward Mars show broad diffuse emission at radial velocities expected for the decelerated H I flow in the inner solar system. Clarke et al. (1995) suggested that the broad width of this emission could be due to a dispersion in the flow velocities along this line of sight, but the broad widths could be simply interpreted as thermal broadening with $T = 30{,}000$ K, which would be consistent with the theoretical models (see, e.g., Williams et al. 1996).

Our analysis of the Lyman-α absorption along the line of sight to α Cen led us to include a warm component with the parameters $T = 29{,}000 \pm 5000$ K, $\log N_{H\,I} = 14.74 \pm 0.24$, and a flow velocity of $v_{H\,I} > -16$ km s^{-1}, which suggests at least a small deceleration relative to the LIC inflow velocity at an angle of 52° relative to the upwind direction (see § 3.3). These parameters are within the range of recent theoretical models and support the basic assumptions and results of the models.

The importance of our measurement of the absorption by warm hydrogen toward α Cen is that for the first time we are measuring the column density of H I along the entire line of sight through the heliosphere, rather than an in situ measurement of scattered H I flux, which may not sample well the H I located in the heliosphere far from the Sun where the solar Lyman-α flux is low. Also, there is no confusion with possible diffuse Galactic emission or uncertainties concerning the solar Lyman-α flux. Our data provide the first direct measurement of the temperature of the compressed and heated interstellar H I in the hydrogen wall that can be used to constrain the theoretical models. α Cen is particularly well suited for studying the hydrogen wall because (1) the stars lie in the upwind direction where the wall is predicted to be (whereas stars previously observed by the GHRS all lie in the downwind direction); (2) the interstellar hydrogen column is very low, so the interstellar absorption is narrow enough to not obliterate absorption by warm hydrogen in the wall; and (3) α Cen A and α Cen B are bright enough in the UV to provide high S/N spectra. Lyman-α spectra for other lines of sight should be studied to confirm our conclusions.

4.6. *Astronephography of the LIC*

While α Cen is probably located inside the G cloud, the other stars observed by the GHRS, such as Procyon and Capella, probably lie outside the LIC, which is also a warm, neutral cloud (Lallement et al. 1995). We can use the knowledge that α Cen lies within the G cloud to estimate the mean H I density along this line of sight. Our value of $\log N_{H\,I} = 17.80 \pm 0.30$ corresponds to $n_{H\,I} = 0.15$ cm^{-3} with an uncertainty of a factor of 2. To our knowledge, this is the first direct measurement of the H I density within a local cloud, rather than an inference of $n_{H\,I}$ on the basis of Lyman-α scattered emission inside the heliosphere and theoretical models of the solar wind and interstellar gas interaction.

If we adopt the value 0.15 cm^{-3} as representative of the H I density in the G cloud and the LIC, we can estimate the distance to the edge of the LIC (d_{edge}) in the direction of Procyon, Capella, and other stars. We find that the distance to the edge of the LIC is only 3.9 pc toward Capella and

only 2.5 pc toward Procyon. Since the distance to Procyon is 3.5 pc, there is room for the second cloud detected along this line of sight (see Paper II) to lie outside of the LIC. These values for d_{edge} are uncertain because of the factor of 2 uncertainty in the H I density in the G cloud and the assumption that the densities of the G cloud and the LIC are the same.

Accurate measurements of the H I column toward other stars obtained with the GHRS are now becoming available. For example, Gry et al. (1995) found that component 1 in the line of sight toward ϵ CMa has the local cloud velocity and $\log N_{H\,I} = 17.34$. The hot white dwarf G191 − B2B shows a component (called cloud B) with the local cloud velocity and $\log N_{H\,I} = 18.27$ (Lemoine et al. 1995). Also, Frisch (1994) has estimated that component 1 along the line of sight to Sirius is mostly ionized with a total column of 5.1×10^{17} cm^{-2}. By using the same technique as before, we estimate the distance to the cloud edge toward each star to be 0.47 pc (ϵ CMa), 4.0 pc (G191 − B2B), and 1.1 pc (Sirius). Since Sirius is at a distance of 2.7 pc, there is room for the second cloud along its line of sight (see Lallement et al. 1994) to lie outside of the LIC.

With five distances to the edge of the LIC in different directions, we can begin to draw the surface of the local cloud. Frisch (1994) and Lallement et al. (1995) began this morphological study by using inferred rather than measured values of $n_{H\,I}$. As more diverse lines of sight are studied, we can construct a three-dimensional representation of the cloud. Since this is a new field of study, it requires a new name. In analogy with "geography," we propose the name "astronephography" based on the Greek word $\nu\epsilon\phi o\sigma$ (nephos), meaning "cloud."

5. CONCLUSIONS

We summarize here the results of our analysis of GHRS echelle spectra of interstellar absorption in the short (1.34 pc) lines of sight toward α Cen A and α Cen B:

1. The interstellar absorption features detected in the resonance lines of Mg II, Fe II, and D I all have the same heliocentric velocity ($v = -18.0 \pm 0.2$ km s^{-1}), which is consistent with the flow vector for the G cloud proposed by Lallement & Bertin (1992). The temperature and nonthermal velocity inferred from these line profiles are $T = 5400 \pm 500$ K and $\xi = 1.20 \pm 0.25$ km s^{-1}, respectively. The temperature is significantly lower than the 7000 K value previously obtained for the Capella and Procyon lines of sight that extend through the outer edge of the local interstellar cloud (LIC). The turbulent velocity toward α Cen is the same as that found for the Procyon line of sight and is very subsonic. The lower temperature toward α Cen could result from the G cloud being more shielded from ionizing flux from hot stars such as ϵ CMa located outside of the LIC or perhaps could indicate a lower dust/gas ratio in the G Cloud.

2. Our single-component fits to the H I lines suggest $\log N_{H\,I} = 18.03 \pm 0.01$ and $D/H = (5.7 \pm 0.2) \times 10^{-6}$. We had hoped that the very short lines of sight toward α Cen A and α Cen B would contain gas with only one set of physical parameters (e.g., flow velocity, temperature, and turbulent velocity), but we found that the H I absorption is broader than expected from the other lines with a Doppler parameter ($b_{H\,I} = 11.80$ km s^{-1}), which implies a significantly warmer temperature of 8350 K. Furthermore, the velocity of the H I absorption ($v = -15.8 \pm 0.2$ km s^{-1}) is redshifted by about 2.2 km s^{-1} with respect to the velocity of the Fe II, Mg II, and D I lines.

3. The most sensible way to resolve the discrepancy between H I and the other lines is to add a second component to the H I lines. This second component is hotter ($T \approx 30{,}000$ K), is redshifted relative to the primary component by 2–4 km s^{-1}, and has a column density too low to be detected in the Fe II, Mg II, and D I lines. We propose that the gas responsible for this second component is located near the heliopause and is the heated neutral hydrogen from the interstellar medium that is compressed by the solar wind. This so-called "hydrogen wall" is predicted by recent multifluid gasdynamical models of the interstellar gas and solar wind interaction. Our data provide the first measurements of the temperature and column density of H I in the hydrogen wall. Our estimates of the parameters of the solar hydrogen wall are $\log N_{H\,I}^{(2)} = 14.74 \pm 0.24$, $b_{H\,I}^{(2)} = 21.9 \pm 1.7$ km s^{-1} (corresponding to a temperature of $T = 29{,}000 \pm 5000$ K), and $v_{H\,I}^{(2)} > -16$ km s^{-1}.

4. Unfortunately, the existence of this heated H I compromises our ability to compute the H I column density of the interstellar medium accurately because, with slight alterations to our assumed stellar Lyman-α emission line profiles, acceptable two-component fits also exist with $\log N_{H\,I} \sim 17.6$. We, therefore, quote large error bars for the hydrogen column density along the α Cen line of sight: $\log N_{H\,I} = 17.80 \pm 0.30$, $n_{H\,I} = 0.076$–0.30 cm^{-3}, and $D/H = (0.5$–$1.9) \times 10^{-5}$. This range in D/H is consistent with the value $D/H = 1.6 \times 10^{-5}$ previously derived for the Capella and Procyon lines of sight. With the large range of acceptable D/H-values, we cannot tell whether the D/H ratio varies or is constant in the local interstellar medium, but we do find that the D I/Mg II ratio for the α Cen line of sight is about 4 times smaller than for the Capella and Procyon lines of sight. Therefore, either D/H or the Mg depletion varies significantly over distance scales of only a few parsecs. The known variations in the Mg II depletions in the interstellar medium suggest that the Mg II depletion is different for the α Cen line of sight, in which case D/H would be the same as for the Capella and Procyon lines of sight.

5. Since α Cen lies inside the G cloud, we estimate the mean density for this line of sight to be $n_{H\,I} = 0.15$ cm^{-3} with an uncertainty of a factor of 2. This is the first direct measurement of $n_{H\,I}$ in a nearby interstellar cloud, since the other stars observed by the GHRS likely lie outside the LIC. We can use the H I density in the G cloud to estimate the distances to the edge of the LIC along the lines of sight to Capella, Procyon, Sirius, G191 − B2B, and ϵ CMa. These distances provide a rough outline for the LIC and the beginning of "astronephography" as a field of research.

This work is supported by NASA Interagency Transfer S-56460-D to the National Institute of Standards and Technology. We wish to thank V. B. Baranov, Priscilla Frisch, Rosine Lallement, and Lance Williams for sharing their expertise and for sending to us preprints of their recent papers, which were very useful. We also thank Blair Savage for his helpful comments on the manuscript.

REFERENCES

Adams, T. F., & Frisch, P. C. 1977, ApJ, 212, 300
Anders, E., & Grevesse, N. 1989, Geochim. Cosmochim. Acta, 53, 197
Baranov, V. B., Lebedev, M. G., & Malama, Y. G. 1991, ApJ, 375, 347
Baranov, V. B., & Malama, Y. G. 1993, J. Geophys. Res., 98, no. A9, 15157
———. 1995, J. Geophys. Res., 100, no. A8, 14755
Basri, G. S., Linsky, J. L., Bartoe, J.-D. F., Brueckner, G., & Van Hoosier, M. E. 1979, ApJ, 230, 924
Brandt, J. C., et al. 1994, PASP, 106, 890
Brekke, P., Kjeldseth-Moe, O., Bartoe, J.-D. F., & Brueckner, G. E. 1991, ApJS, 75, 1337
Bruston, P., Audouze, J., Vidal-Madjar, A., & Laurent, C. 1981, ApJ, 243, 161
Cerruti-Sola, M., Cheng, C.-C., & Pallavicini, R. 1992, A&A, 256, 185
Clarke, J. T., Lallement, R., Bertaux, J.-L., & Quémerais, E. 1995, ApJ, 448, 893
Dupree, A. K., Baliunas, S. L., & Shipman, H. L. 1977, ApJ, 218, 361
Ferlet, R., Lecavelier, A., Vidal-Madjar, A., Bertin, P., Deleuil, M., Gry, C., Lagrange-Henry, A.-M., & Lallement, R. 1995, A&A, 297, L5
Frisch, P. C. 1994, Science, 265, 1423
———. 1995, Space Sci. Rev., 72, 499
Gilliland, R. L. 1994, GHRS Instrument Science Report 063 (Baltimore: STScI)
Gry, C., Lemonon, L., Vidal-Madjar, A., Lemoine, M., & Ferlet, R. 1995, A&A, 302, 497
Heap, S. R., et al. 1995, PASP, 107, 871
Heiden, A. E. 1988, J. Geophys. Res., 88, no. A12, 10170
Heintz, W. D. 1982, Observatory, 102, 42
Hirshfeld, A., Sinnott, R. W., & Ochsenbein, F. 1991, Sky Catalogue 2000.0, Vol. 1 (Cambridge: Cambridge Univ. Press)
Jenkins, E. B. 1987, in Interstellar Processes, ed. D. H. Hollenbach & H. A. Thronson, Jr. (Dordrecht: Reidel), 533
Jenkins, E. B., Savage, B. D., & Spitzer, L. 1986, ApJ, 301, 355
Lallement, R., & Bertaux, J.-L. 1990, A&A, 231, L3
Lallement, R., Bertaux, J.-L., & Clarke, J. 1993, Science, 260, 1095
Lallement, R., & Bertin, P. 1992, A&A, 266, 479
Lallement, R., Bertin, P., Ferlet, R., Vidal-Madjar, A., & Bertaux, J. L. 1994, A&A, 286, 898
Lallement, R., Ferlet, R., Lagrange, A. M., Lemoine, M., & Vidal-Madjar, A. 1995, A&A, 304, 461
Landsman, W. B., Henry, R. C., Moos, H. W., & Linsky, J. L. 1984, ApJ, 285, 801
Landsman, W. B., Murthy, J., Henry, R. C., Moos, H. W., & Russell, J. L. 1986, ApJ, 303, 791
Landsman, W., & Simon, T. 1993, ApJ, 408, 302
Lemoine, M., Vidal-Madjar, A., Ferlet, R., Bertin, P., Gry, C., & Lallement, R. 1995, in The Light Element Abundances, ed. P. Crane (Berlin: Springer), 233
Linsky, J. L., et al. 1993, ApJ, 402, 694 [Paper I]
Linsky, J. L., Diplas, A., Wood, B. E., Brown, A., Ayres, T. R., & Savage, B. D. 1995, ApJ, 451, 335 [Paper II]
Mewe, R., Kaastra, J. S., Schrijver, C. J., van den Oord, G. H. J., & Alkemade, F. J. M. 1995, A&A, 296, 477
Quémerais, E., Bertaux, J.-L., Sandel, B. R., & Lallement, R. 1994, A&A, 290, 941
Quémerais, E., Sandel, B. R., Lallement, R., & Bertaux, J.-L. 1995, A&A, 299, 249
Robinson, R. D., Blackwell, J., Feggans, K., Lindler, D., Norman, D., & Shore, S. N. 1992, A User's Guide to the GHRS Software, Version 2.0 (Greenbelt: Goddard Space Flight Center)
Soderblom, D. R., Hulbert, S. J., Leitherer, C., & Sherbert, L. E. 1994, *HST* Goddard High Resolution Spectrograph Instrument Handbook, Version 5.0 (Baltimore: STScI)
Sofia, U. J., Cardelli, J. A., & Savage, B. D. 1994, ApJ, 430, 650
Vladilo, G., Molaro, P., Crivellari, L., Foing, B. H., Beckerman, J. E., & Genova, R. 1987, A&A, 185, 233
Williams, L. L., Hall, D. T., Pauls, H. L., & Zank, G. P. 1996, in Proc. Solar Wind 8 Workshop, in press
Wilson, O. C., & Bappu, M. K. V. 1957, ApJ, 125, 661
Witte, M., Rosenbauer, H., Banaszkewicz, M., & Fahr, H. 1993, Adv. Space Res., 13, no. 6, 121
Wolfire, M. G., Hollenbach, D., McKee, C., Tielens, A. G. G. M., & Bakes, E. L. O. 1995, ApJ, 443, 152
Zank, G. P., Pauls, H. L., Williams, L. L., & Hall, D. T. 1996, in Proc. Solar Wind 8 Workshop, in press